Utrecht University

Debye Institute For Nanomaterials Science

Soft Condensed Matter

Master Thesis
Nanomaterials Science

Fully Biobased Size-Tunable UV-Absorbing Nanoparticles for Photoprotection

By

Heleen Kibbelaar

Under supervision of

Douglas R. Hayden
Dr. Arnout Imhof
Prof. Dr. Krassimir P. Velikov

2 February 2018

Abstract

There is a growing interest in developing products from biobased and environmentally friendly material. In particular, the use of biobased materials in the development of functional nanoparticles can result in novel and high performance materials with an entirely biobased composition. In this work, we explore the two biopolymers ethyl cellulose and zein for the preparation of biobased functional nanoparticles. We first explore the synthesis of nanoparticles from ethyl cellulose via an upscalable synthesis technique and find that the particle size can be tuned between 50 and 165 nm.

We then investigate these ethyl cellulose nanoparticles, and nanoparticles from another biopolymer (zein), as carriers for biobased photoprotectants (quercetin, retinol, and *p*-coumaric acid) for applications in photoprotection. The prepared biobased photoprotective nanoparticles from ethyl cellulose/zein with encapsulated biobased photoprotectants have the potential to satisfy both environmental and health issues, currently encountered, in photoprotection. We found that the composition of these biobased photoprotective nanoparticles could easily be tuned and the nanoparticles could prepare effective, UV-absorbing, transparent coatings.

The findings in this work show the excellent potential for photoprotective nanoparticles from ethyl cellulose and zein in photoprotection applications, because of their easy tunability in size and composition, upscalable potential and biobased and environmentally friendly composition. These results also have significant implications for the more general field of functional nanoparticles.

Table of Contents

List of abbreviations

C	*p*-coumaric acid
Cryo-EM	Cryo- Electron Microscopy
DLS	Dynamic Light Scattering
EC	Ethyl Cellulose
ECNP	Ethyl Cellulose Nanoparticle
FTIR	Fourier Transform Infrared Spectroscopy
PDI	Poly Dispersity Index
Q	Quercetin
R	Retinol
SEM	Scanning Electron Microscopy
TEM	Transmission Electron Microscopy
ZNP	Zein Nanoparticle

General Introduction

Nanoparticles are becoming increasingly popular as building blocks for novel functional materials. The promising benefits of nanotechnology have been employed by many industries, and commercial products are already being fabricated, such as in the microelectronics[1], pharmaceutical[2–4], food[5–7] and cosmetic industry[8–10].

Techniques used to prepare nanoparticles can be classified as top-down methods (such as homogenization and milling) or bottom-up methods (such as spontaneous emulsification or anti-solvent precipitation). For a nanoparticle preparation technique to be commercially viable, the technique should be cost-effective and therefore be easily upscalable for industrial processes[7]. One promising upscalable technique for the development of nanoparticles for commercial applications is the anti-solvent precipitation method.

The antisolvent precipitation technique can be used to prepare nanoparticles from a broad variety of polymeric materials. The preparation of nanoparticles from polymeric materials is particularly attractive because many polymers from a biobased source exist. This means that nanoparticles can be prepared which are attractive for use in food, pharmaceutical and cosmetic applications[6]. There is growing interest in the use of biopolymer materials due to concerns about limited natural resources of fossil fuel reserves and move to sustainable materials basis[11,12]. Such biopolymer material includes starches, cellulose derivatives, chitosan/chitin, gums, proteins (animal or plant-based) and lipids[13]. These materials offer extra advantages such as abundancy in nature, edibility, biodegradability, aesthetic appearance, non-toxicity, non-polluting and low cost[14].

More recently, there has been increasing focus on the development of specifically designed biopolymer nanoparticles with functionality, for example for use in drug delivery systems[3] and for optical applications[6]. The incorporation of optically active molecules into nanoparticles (bio-nanocomposites), in particular, has significant importance in applications such as displays[15,16], sensors,[15,17] pigments,[18] and sunscreens[19–21].

Concerning sunscreen applications, recent work of Hayden *et al*.[22] showed that nanoparticles of the biopolymer ethyl cellulose (EC) are effective in the encapsulation of synthetic UV absorbing molecules in sunscreens. The encapsulation of synthetic organic UV filters into biobased nanoparticles has the potential to address current issues in photoprotection regarding skin contact with the potential carcinogenic synthetic organic UV filters. Moreover, they showed that antioxidants can be co-encapsulated into the nanoparticles in order to neutralize any harmful degradation products formed as a result of the degradation of the synthetic organic UV filters. Despite progress, the adverse health effects associated with the use of synthetic organic UV filters in sunscreens cannot be completely eliminated, and these synthetic organic UV filters are also known to be potentially hazardous to the environment[23]. Therefore, the replacement of synthetic organic UV filters with biobased UV-absorbing photoprotectants obtainable from plants – which are potentially safer – and encapsulation into nanoparticles from biopolymers such as EC and zein has the potential to satisfy both health and environmental concerns in photoprotection. Besides, the creation of a fully biobased and edible system also opens up opportunities to apply the system in food packaging material for photoprotection, whereas non-edible synthetic filters cannot be used for this purpose.

Here, we explore the preparation of all-natural UV-absorbing nanoparticles from the biopolymers EC and zein with encapsulated biobased photoprotectants. Firstly, we prepare ethyl cellulose nanoparticles (ECNPs) using an upscalable anti-solvent precipitation method and explore the range of particle size tunability. The tunability in size of the particles is important to study because smaller nanoparticles have different physicochemical and physiological properties than larger particles, such as reduced light scattering, which is appealing for the use of these nanoparticles in cosmetic formulations. Thereafter, we quantify the encapsulation of biobased photoprotectants into ECNPs and zein nanoparticles (ZNPs) and explore the preparation of effective, transparent, UV-absorbing coatings from these all-natural nanoparticles. These results have significant implications in the fields of photoprotection and functional nanoparticles.

1

Size Tunable Ethyl Cellulose Nanoparticles

Biopolymer nanoparticles are frequently used in food, pharmaceutical and cosmetic products for their unique and novel properties. The size of a nanoparticle significantly determines the quality and properties of the final product and it is therefore important to control the size of the nanoparticle. In this chapter the possible size range of nanoparticles prepared from the biopolymer ethyl cellulose through an antisolvent precipitation method are explored. In the antisolvent precipitation method, ethyl cellulose nanoparticles are prepared by dissolving ethyl cellulose in ethanol before pouring this solution into an antisolvent water. The ethyl cellulose nanoparticles were tunable in size between 50 and 165 nm by increasing the amount of dispersed polymer in the ethanol solution. Attempts to prepare bigger particles (than 165 nm) resulted in bimodal particle size distributions, while attempts to prepare smaller particles (than 50 nm) did not result in the formation of particles. The growth in particle size follows a positive linear trend with EC concentration and a nucleation and aggregation mechanism instead of a classical nucleation growth mechanism is therefore assumed.

1 Introduction

Nanoparticles are finding increasing application as ingredients in food, cosmetic and pharmaceutical products due to their particular physicochemical properties and functional attributes[24]. The small size of nanoparticles means that they have different physicochemical and physiological properties than larger particles, such as reduced light scattering, improved stability to gravitational separation and aggregation, faster diffusion rates, higher solubility, and higher penetration rates through biological barriers[6]. The high surface/volume ratio increases the importance of the properties of the surface molecules over the bulk molecules[25,26].

Processing of fine particles is one of the most important outcomes for many formulation technologies and the quality of the final product is often significantly affected by the size distribution and the shape of the particles used in material formulation. While many methods are available for synthesizing nanoparticles in dispersion, understanding the precipitation processes and possibility of methods to scale these reactions up to commercial scale remains limited[27,28].

The anti-solvent precipitation, also known as nanoprecipitation or phase separation, has drawn increased interest due to its simplicity, upscalable potential and particle size tuning/preparation of fine particles. The anti-solvent precipitation method is involved during three processes of the particle formation: clustering, nucleation, and nucleus growth[29,30]. The solute concentration, mixing method, solvent/anti-solvent ratio and compositions, and the absence/presence of additives may exert various effects on the previously mentioned processes and therefore may affect the properties of the resultant particles, such as size, size distribution, and surface characteristics[28].

Ethyl cellulose nanoparticles (ECNPs) prepared by the anti-solvent precipitation method have shown to be promising in the stabilization of liquid/liquid[31] and air/liquid[32] interfaces as well as being efficient in the encapsulation of active materials[22,33,34]. Furthermore, ethyl cellulose (EC) is attractive for food and cosmetic applications because of its food grade properties[32].

The solubility physical properties of EC make it a suitable biopolymer for the production of nanoparticles by the anti-solvent method (soluble in ethanol and insoluble in water). As the dimensions of a biopolymer particle alter its functional performance in fields as foods, cosmetic and pharmaceutics the particle size has to be precisely controlled[6].

In order to expand the possibilities to use ECNPs for the encapsulation of active ingredients, the range of particle sizes which can be prepared using the simple up-scalable ‘antisolvent precipitation’ method is explored in this chapter. After a theory section which includes the anti-solvent precipitation method and its most important parameters, the possible range of particle sizes is studied by the use of characterization techniques such as dynamic light scattering (DLS) and electron microscopy imaging.

2 Theory

2.1 Anti-solvent precipitation

The anti-solvent precipitation technique is suitable for producing nanoparticles from a range of different proteins and polysaccharides and is especially used for insoluble polymer materials[35–38]. This technique favours the production of very fine particles with an improved control over particle properties, such as size, morphology and physical state. Anti-solvent precipitation is an appealing technology as no specialized equipment and complex operating conditions are needed. Besides, the related costs are reasonably low, the technique is easily up-scalable and sample contamination is often less significant than when using top down technologies[39]. The anti-solvent precipitation technique is already frequently used to produce nanoparticles for pharmaceutical purposes[40].

Anti-solvent precipitation can be attained by addition of a non-solvent to a solution, hence, inducing supersaturation, which provides a driving force for solute precipitation. Careful and proper selection of the solvent and anti-solvent is required, where the nature of the biopolymers or compounds used to produce the nanoparticles has to be taking into account. A number of liquids are commonly used as both solvents and anti-solvents, such as water, organic solvents or supercritical CO_2[41]. The selected solvents and antisolvent need to be miscible over the concentration range at which they will be used during the production of the nanoparticles.

The imbalance of molecular interactions between solute, solvent and anti-solvent is the main driving force for the formation of particles during anti-solvent precipitation. Precipitation occurs when the solute-solute interactions are strong enough to overcome other interactions and entropy of mixing effects which occurs at certain solvent/anti-solvent combinations. Sufficiently strong repulsion between the particles prevents them from aggregation. Different production stages can be distinguished in the anti-solvent precipitation process: mixing of solution and anti-solvent, generation of supersaturation; nucleation; particle growth; and, coagulation.

2.1.1 Supersaturation and nucleation

During an antisolvent precipitation of a poorly water-soluble solute, the solute is first dissolved in a solvent and then rapidly mixed with an antisolvent (e.g., water). The addition of the solution to the anti-solvent lowers the solubility of the solute compared to that in the original solvent. In this way, a driving force for precipitation, called supersaturation is created, which is defined as:

$$S = \frac{c}{c_{eq}} \tag{1}$$

where c is the initial solute concentration in the solution to be precipitated and c_{eq} is the equilibrium solubility of the solute in a mixture of organic solvent and antisolvent.

For the nucleation to occur, supersaturation is a prerequisite. Several types of nucleation can be distinguished based on the presence or absence of foreign particles or surfaces that promote nucleation, i.e. heterogeneous or homogeneous nucleation, respectively. In what follows, homogeneous nucleation is considered.

The Gibbs free energy change, ΔG, is the thermodynamic parameter that indicates whether nucleation is possible or not. It is represented as the energy barrier that has to be overcome to form nuclei:

$$\Delta G = \frac{16\pi\gamma^3 V_s^3}{3k^2T^2(lnS)^2} \quad (2)$$

where γ is the surface tension, V_s is the molecular volume (molar volume/Avogadro number), k is the Boltzmann constant, T is the absolute temperature, and S is the supersaturation.

The energy barrier for particle precipitation from saturated solution depends on the metastable zone width. The metastable zone width is the range of solvent/anti-solvent compositions in which no nucleation is observed within a given time frame. If high and homogenous nucleation rates are desired the metastable zone width should be short[7,39].

According to equation 2, up to a critical solute concentration, a higher supersaturation (S) and lower surface tension (γ) decrease the critical energy barrier (ΔG), which should lead to fast nucleation and hence the production of more and smaller particles[42,43].

The kinetic parameter describing how fast the nucleation occurs is given by the rate of nucleation per unit volume and per unit time, R_N, as:

$$R_n = \left\{\frac{CkT}{3\pi\lambda^3\eta}\right\} exp\left(-\frac{\Delta G}{kT}\right) \quad (3)$$

where λ is the diameter of the growth species and η is the viscosity of the solution. This equation indicates that a high initial concentration (C) or a higher supersaturation (i.e., a large number of nucleation sites), low viscosity (η), and low critical energy barrier (ΔG) favours the formation of a large number of nuclei. A larger number of nuclei leaves less solute per nucleus available (if no extra solute is added) and smaller particles are being formed.

Figure 1 schematically illustrates the anti-solvent process of supersaturation, nucleation, and subsequent growth by coagulation and condensation. When the solute concentration exceeds the equilibrium saturation concentration (c_{eq}), the system becomes saturated and above a certain critical supersaturation concentration, nucleation is induced. This corresponds to the energy barrier defined by equation 2 for the formation of nuclei. After the initial nucleation, the concentration or supersaturation of the growth species decreases. When the concentration decreases below this critical concentration, which corresponds to the critical energy, no more nuclei would form[44]. The formed nuclei keep on growing by either condensation or coagulation.

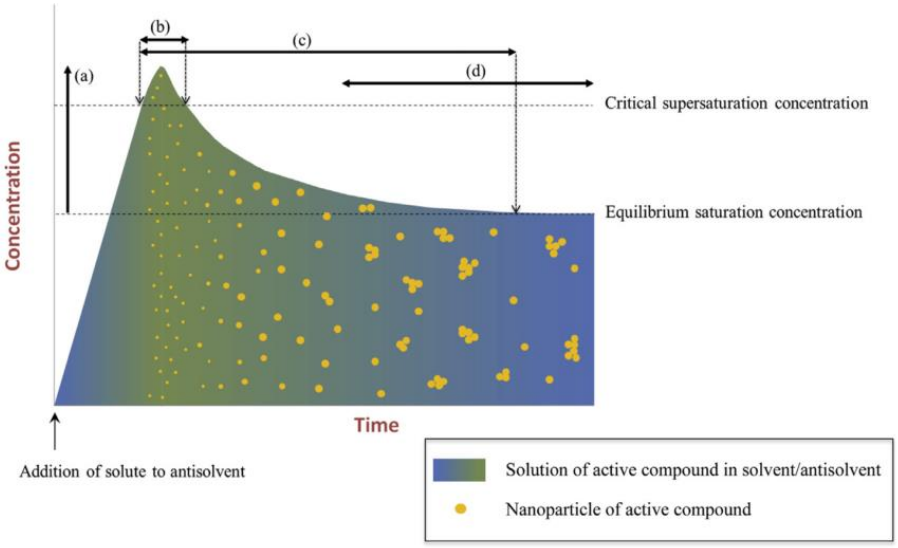

Figure 1: schematic representation of the anti-solvent process. The different stages, i.e. supersaturation (a), nucleation (b), particle growth by condensation (c) and by coagulation (d) are indicated on the scheme[7].

2.1.2 Nuclei growth through condensation

Condensation is defined as the addition of single molecules to the particle surface, whereas coagulation occurs when two or more particles collide and stick together, forming bigger particles. Particle growth through condensation continues until the free (non-absorbed) solute concentration reaches the equilibrium saturation concentration (Figure 1)[43,45]. Condensation reduces supersaturation by decreasing the mass of solute in the solution and, therefore, competes with nucleation. The rate of condensation is decreased by coagulation as the total number of particle and therefore the surface area are reduced[46].

Supersaturation controls the nucleation and growth rates to different extents. The nucleation rate depends more strongly on S, as shown in equation 3, than does the rate of condensation, which is linear in S[47]. High nucleation rates enable to produce a large number of submicrometer particles in the final suspension, if the growth can be delayed[43].

2.1.3 Particle growth through coagulation

Particle coagulation is another major driving force for particle growth when the solute concentration is lower than the equilibrium saturation concentration (Figure 1). Particle coagulation is favoured when the attractive interactions (such as van de Waals and hydrophobic interactions) dominate the repulsive interactions (such as steric or electrostatic repulsion). The particles within an aggregate may maintain their individual shapes. Application of mechanical forces, such as stirring, homogenization, or ultrasonic treatment can sometimes cause the release of the particles. On the contrary, particles may be difficult to separate when the particles fuse together after aggregation[40]. The kinetics of particle coagulation depends on the collision frequency and efficiency. The collision frequency is defined as the number of collisions per unit time, which depends on particle size, particle concentration, and particle motion (e.g., Brownian, gravitational, or mechanical). The collision frequency is described as the number of collisions that lead to coagulation, and is a balance between attractive and repulsive interactions operating between the particles. Stabilization of the particles against coagulation can be achieved by inclusion of stabilizing agents in the production process. Stabilizing molecules adsorb to the surface of the nanoparticles and improve stability by introducing repulsive interactions, such as steric or electrostatic repulsion[48].

2.2 Important Parameters for anti-solvent precipitation

The control of particle size distribution and stability of ultrafine particles produced by anti-solvent precipitation is crucial for many commercial applications[39]. Fine particles with a low polydispersity index that have a good stability and gravitational separation are typically preferred by manufacturers. The parameters of particle growth experiments strongly influence the mechanism of particle formation and govern the form of crystal size and its distribution[49]. The most important parameters for the research in this thesis are briefly discussed below.

Mixing

The stirring speed has an effect on the mixing phenomena between solvent to anti solvent which leads to a reduction in the solubility of solute in a solvent. An overall observation is that increasing the stirring speed decreases the size of the particles. Increasing the micromixing efficiency boosts the mass transfer and the rate of diffusion between the multiphases. This results into a high homogenous supersaturation, which activates the rapid nucleation to produce smaller particles[50].

Addition of solute to anti-solvent

The addition speed and order (solvent to anti-solvent or anti-solvent to solvent) have a significant impact on the particle properties. These two parameters strongly influence the nucleation rate and particle growth kinetics as they determine the rate and degree of supersaturation. Kakran *et al.*[51] found that the dimensions of curcumin nanoparticles significantly reduce by increasing the flow rate of a curcumin solution into an anti-solvent. Likewise, Park *et al.*[52] reported that an effect on particle size and shape was observed, when the injection rate of the anti-solvent, in this case supercritical CO_2, was adjusted. Langer *et al.*[35], found, on the other hand, that an altering of the addition rate had a significant effect on the polydispersity index of the particles, but not on the particle size. Regarding the addition order, Park *et al.*[52] found that the particle size was larger when the anti-solvent was added to the solute/solvent system than the other way around.

Anti-solvent to solvent ratio

Numerous studies have shown that the particle size can be reduced by increasing the volume of anti-solvent volume used[38,51,53–57]. Zhao *et al.*[54] created danazol nanoparticles using a microchannel reactor and observed an inverse proportional relationship between the anti-solvent-to-solvent ratio and the particle size. Two hypothesis were stated: (i) the instantaneous supersaturation was increased due to the more rapid reduction in solvent concentration[51,54] and, (ii) crystal growth was reduced at lower solute concentrations[54]. After formation of the nuclei, particle growth happens which is partially impeded at higher anti-solvent volumes as the diffusion distance for the growing species expands and the process becomes diffusion limited[51].

Effect of Compound concentration

Following the classical nucleation and growth theory, particle sizes decrease upon an increase in the solute concentration. When the compound concentration is increased, the degree of supersaturation can alter the rate of nucleation. A high rate of nucleation is responsible for the creation of a large number of nuclei, which leads to the increase in the number of crystals and hence, it could make the size of each crystal smaller. However, an increase in the

concentration, could also lead to agglomeration during the course of the precipitation which may lead to a poor distribution in both size and shape of the final product. Large number of nuclei decreases the diffusion from solvent to antisolvent and lead to particle aggregation[50]. An increase in the viscosity of the drug solution hinders the drug diffusion between solution and antisolvent and results in non-uniform supersaturation and agglomeration. An increase in particle size was also found by Rossi *et al.*[58] and Zhang *et al.*[59] for nanoparticles of phytosterol and cefuroxime, respectively.

Selection of an appropriate (anti-)solvent

The nature of the used anti-solvent is extremely crucial in controlling the precipitation process. Essential for the anti-solvent is its (non) solubility towards the solvent phase in which the solute of interest is dissolved. Several research pointed out that particle size and morphology depend strongly on the solubility parameters of the solvent and anti-solvent[59,60]. The flow behaviour of the solvent and the anti-solvent, and the physicochemical properties of both liquids, determine the mixing behaviour of the solvent and anti-solvent. Besides, the nature of the anti-solvent also alters the structure of the formed crystals[7].

2.3 Ethyl Cellulose

Ethyl cellulose is made by chemical substitution of the naturally occurring polymer, cellulose which is the most abundant organic compound on earth. The chemical structure of EC is depicted in Figure 2.

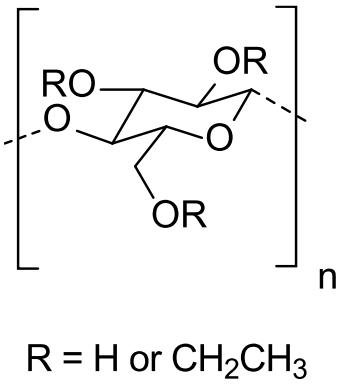

$R = H \text{ or } CH_2CH_3$

Figure 2: chemical structure of Ethyl Cellulose.

The molecule has a structure of repeating anhydroglucose (cellulose) units, where a high degree of hydroxy-groups on the anhydroglucose are etherified with ethyl-groups. The -OH groups of cellulose can partially or fully react with various chemicals to provide derivatives with useful properties[61]. EC is prepared from wood pulp or cotton by treatment with alkali and ethylation of the alkali treated cellulose with ethyl chloride, where the number of ethyl groups can vary depending on the manufacture. The average number of cellulose hydroxyls substituted (by ethoxyl groups) determines the degree of substitution and thus also its solubility properties. EC is hydrophobic in nature and used extensively as a coating material, as a tablet binder, in microcapsules and microspheres and to prepare controlled delivery systems.

3 Experimental details

3.1 Materials

Ethyl cellulose (EC) degree of substitution 2.1-2.6 (100 cP, lot number MKBT0521V) was purchased form Sigma Aldrich. Ethanol (100%) was purchased from Interchema and pure water was used from a Millipore system.

3.2 Methods

Preparation of ECNPs

ECNPs were synthesized via an 'antisolvent precipitation' method from literature[31]. A series of different sizes of ECNPs were prepared by dissolving various masses of EC (0.08 g, 0.1 g, 0.1375 g, 0.275 g, 0.5 g, 0.75 g, 1 g, 1.125 g, 1.25 g) in ethanol (50 mL) before pouring into the antisolvent water (150 mL, pH 5-6) under fast magnetic stirring, resulting in the spontaneous formation of ECNPs. The procedure is schematically depicted in Figure 3.

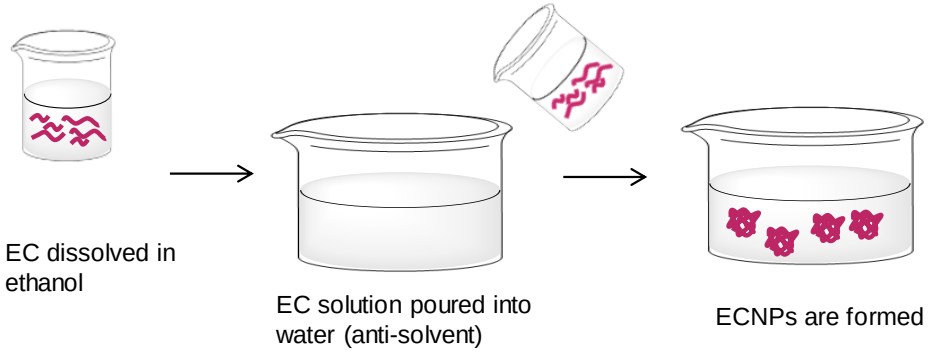

Figure 3: schematic representation of the preparation of ECNPs via the anti-solvent precipitation method.

Ethanol and some water was removed by rotary evaporation. If too much water was evaporated, water was added to the dispersion up to 50 mL in order to keep particles concentrations consistent. The resulting dispersions were filtered with a 1.2 µm filter to remove any large aggregates formed during the antisolvent precipitation.

3.3 Characterization

Particle size determination

Size characterization of ECNPs and ZNPs was done with TEM (Philips TECNAI12 electron microscope, samples prepared by pipetting a drop of the ECNP dispersion onto a Butvar-coated TEM grid), SEM (FEI XL30FEG), and DLS (Malvern Zetasizer Nano ZS, particle size distributions were obtained by using a Contin algorithm).

Yield determination

The yield of ECNPs for the series in which increasing concentrations of EC in ethanol solution were used was quantified (particles formed mass/mass of EC originally added x 100). Yield values were determined by taking 10 mL of the dispersion and drying in a glass vial at 80 ºC overnight. The mass of the dried particles was then measured, multiplied by 5 (to correspond to the total 50 mL dispersion), and then this value was divided by the initial mass of EC added. This was done two-fold.

4 Results and Discussion

Preparation of ECNPs and Investigation of the Particle Size Tunability

In order to investigate the accessible size range of the ECNPs, using a antisolvent precipitation method from literature[62], different sizes of ECNPs were prepared. The used solvent/anti-solvent (ethanol/water) system is chosen because of the solubility of EC in ethanol and non-solubility in water.

As discussed in the theory section, different parameters can affect the particle size. Plasari *et al.*[28] found that many process parameters, such as the type of stirrer and the stirring speed, the temperature and the solvent-nonsolvent ratio, have practically no influence on the formation of EC particles. The EC concentration in the initial alcoholic solution appeared to be the most important parameter controlling the particle size distribution.

In this work particle sizes were, therefore, tuned by varying the amount of EC during the synthesis (the other parameters such as temperature, mixing speed were kept constant).

Figure 4 shows the average particle sizes as measured by DLS and plotted as a function of EC concentration in Figure 4(i). The complete raw data set for Figure 4 can be found in appendix A. Both the mean and modal average are reported for the particle size for completeness but the plot in Figure 4(i) only uses the values for the mean average particle size.

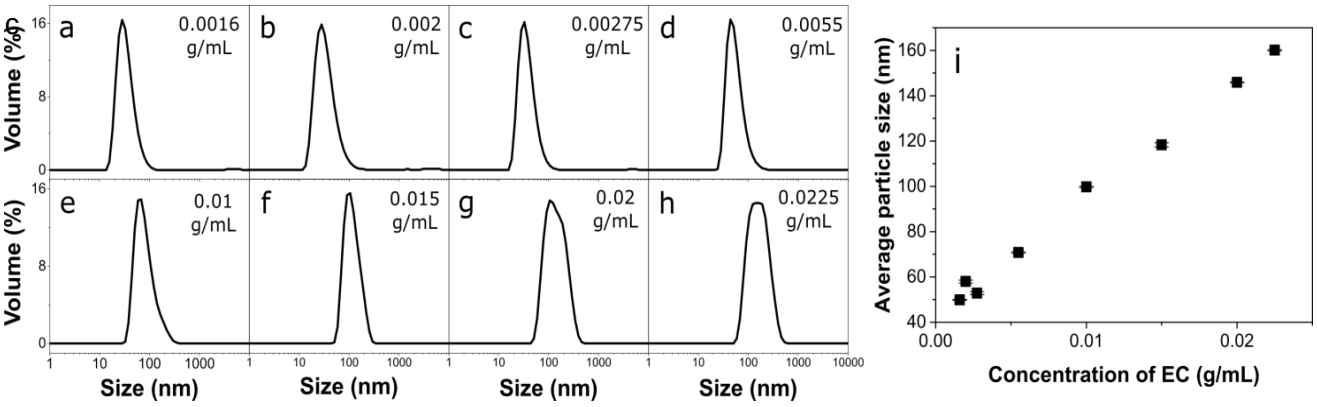

Figure 4: (a-h) volume weighted size distributions determined by DLS for ECNPs at various EC concentrations in ethanol. (i) Average particle size (values from the DLS measurements) as a function of the concentration of EC used in the antisolvent precipitation. The measurements were performed in duplicate to give the error bars in (i).

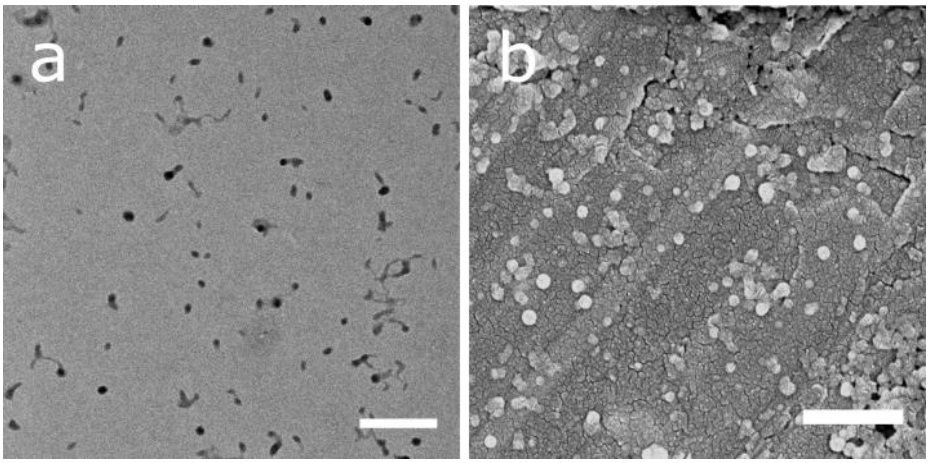

Figure 5: TEM (a) and SEM (b) image of ECNPS. Scale bars 500 nm.

The average size of the ECNPs could easily be tuned between 50 nm and 165 nm in diameter. TEM and SEM imaging showed particle sizes consistent with DLS measurements (Figure 5). Particle sizes were better measurable with SEM imaging because the particles appeared to quench/melt under TEM conditions.

Classical theory of homogenous nucleation suggests that particle sizes decrease upon the increase in supersaturation which occurs when the concentration increases. Interestingly, the plot in Figure 4(i) shows an almost perfect positive linear dependence on the initial concentration of EC in ethanol.

This positive linear increase in particle size, upon concentration increase, is a phenomenon which has been observed with other materials using an antisolvent precipitation method[51,63–65] and several mechanisms are proposed.

For example, Plasari et al.[28] suggest that the rate of nucleation does not depend on the solution concentration, which means that at higher solute concentration more material is accessible for the same amount of nuclei, leading to bigger particles. This is in agreement with the above described experimental results. From the theory of Plasari *et al.* a cubic root dependency is expected for the growth of the particles. To verify whether the observed linear dependency in this work is not a consequence of the concentration regime, the particle sizes wear fitted against a linear and cubic root model.

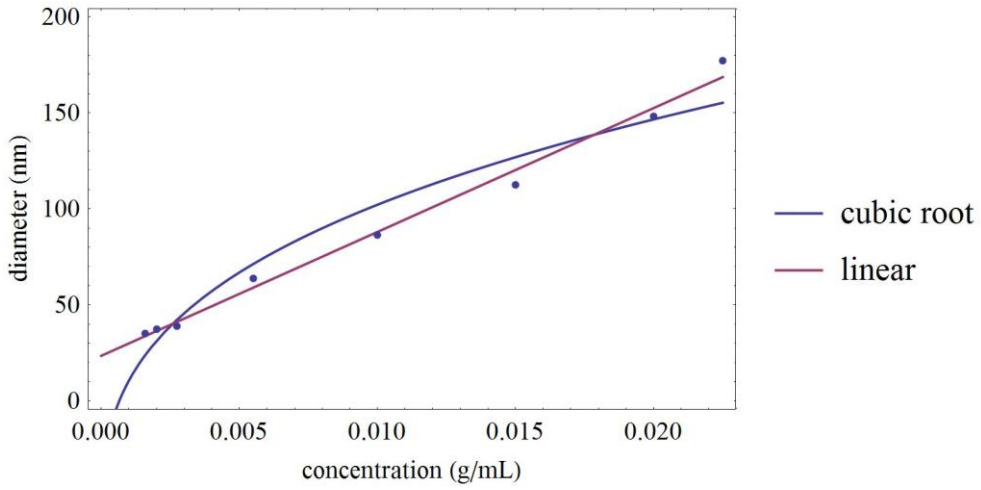

Figure 6: average particle sizes fitted with a linear and cubic root model fit.

Figure 6 shows that the dependency is indeed better described by a linear than cubic root relation. Another confirmation of the linear dependency is the found decrease in number of particles with the concentration, which is depicted in Figure 7 and determined by dividing the volume of all particles in the dispersion by the volume of one particle where the volume of all the particles is determined by dividing the dry mass by the found average diameter. The decrease in number of particles is only possible for linear relations. Whereas, the model of Plasari *et al*. assumes a constant amount of nuclei.

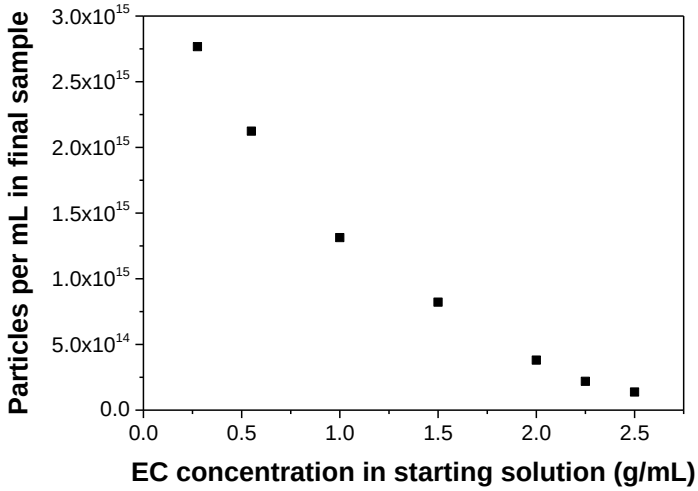

Figure 7: number of particles EC measured in the final sample as a function of the concentration (g/mL).

The nucleation and aggregation mechanism, proposed by several researchers[66–68], seems to be more likely. A higher solute concentration increases the degree of supersaturation, which will lead to the formation of more and smaller nuclei, but, at the same time, nuclei growth will be promoted as the frequency of particle collisions will also go up and the diffusion length will be significantly reduced. Particle agglomeration can also be a result of an increase in viscosity, which will hinder the diffusion between solvent and anti-solvent, leading to non-uniform supersaturation, slower nucleation rates and increased particle agglomeration[51,67].

Attempts to prepare particles smaller than 50 nm by using less than 0.0016 g/mL of EC in ethanol did not result in the formation of particles (particle concentration was too low to be measured by DLS). Aqueous ECNPs dispersions with smaller sizes (42 nm) have actually been reported in literature by using lower EC concentrations and a different solvent system (isopropyl alcohol instead of ethanol)[62]. From Figure 8 can be seen that attempts to prepare particles greater in size than 165 nm (by using 0.025 g/ mL of EC in ethanol) resulted in bimodal, very polydisperse particle size distributions (raw data appendix A).

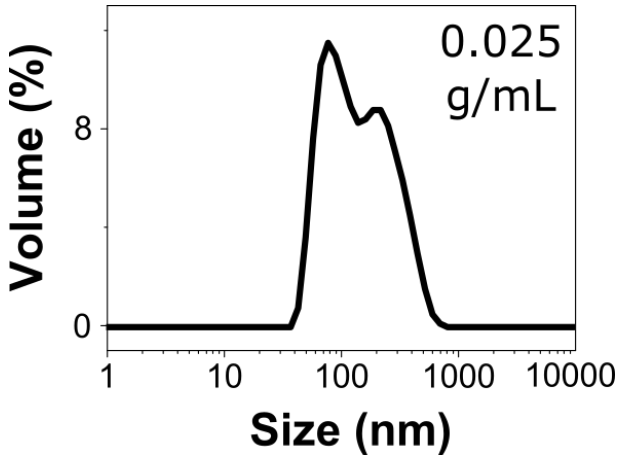

Figure 8: volume weighted size distribution as determined by DLS for when 0.025 g mL^{-1} EC in ethanol is used for the antisolvent precipitation. Note that the DLS measurement shows a very polydisperse bimodal distribution of particles.

During the precipitation reaction of particles greater in size than 165 nm, large amounts of macroscopic aggregates were formed. This tendency, that greater amounts of macroscopic aggregates of precipitated EC formed during the antisolvent precipitation as a function of greater initial EC concentration in ethanol, was actually found in general. This is consistent with the found yield of the (formed) particles. Figure 9 shows the yield percentage of each different particle size, where can be seen that the yield decreases upon increasing concentrations of EC (raw data appendix A).

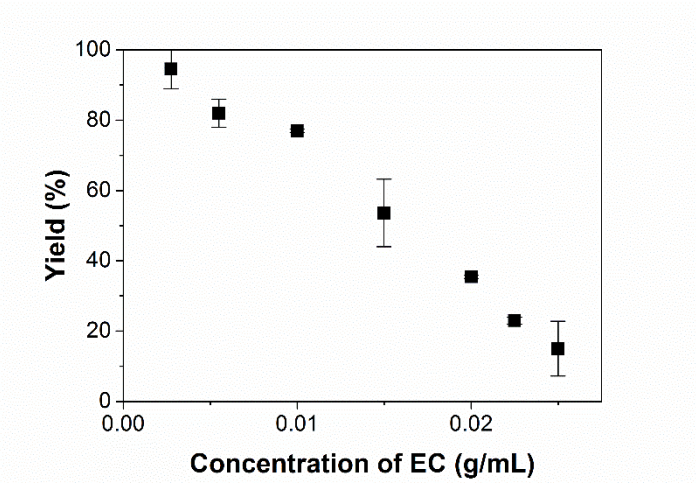

Figure 9: the yield for the series as a function of the concentration of EC in ethanol. The two in the series concerning the lowest two concentrations of EC in ethanol (1.6x10^{-3} g mL-1 and 2×10^{-3} g mL-1) are not measured because the particle sizes for the lowest three concentrations were all similar.

Smaller particles were formed with very high yield (close to 100%), whereas larger particles (>100 nm) were prepared with lower yields. The yield of the larger particles may be increased by the introduction of a steric stabilizer, but this was not tried as it is desirable to keep the formulation as simple as possible.

The complete raw data set for Figure 4, Figure 8, Figure 9 can be found in the appendix. Both the mean and modal average are reported for the particle size for completeness but the graph in Figure 4 only uses the values for the mean average particle size.

5 Conclusion and Outlook

In this chapter we explored the size tunability of ECNPs prepared by an anti-solvent method. The ECNPs were tunable in size between 50 and 165 nm, simply by increasing the amount of dispersed polymer in the ethanol solution. Attempts to prepare bigger particles (than 165 nm) led to a bimodal system, while attempts to prepare ECNPs smaller than 50 nm did not result in the formation of particles. Moreover, we found that the yield decreased for the preparation of bigger particles, which is a consequence of the formation of more precipitation during the anti-solvent precipitation method when bigger particles were tried to prepared.

A positive linear dependency was found for the increase in particle size, which is not typical for the classical theory of homogenous nucleation, but also found for more similar systems using the antisolvent precipitation method. The particle growth may instead follow a nucleation and aggregation mechanism, where the formation of more and smaller nuclei decreases the diffusion from solvent to antisolvent and increases the viscosity leading to particle agglomeration. Cryo-EM experiments could reveal more about the formation mechanism because the particles can then be studied in the liquid phase. With these experiments it might be possible to see whether particles aggregate and therefore increased particle size is observed.

2

All-Natural UV-Absorbing Nanoparticles for Environmentally Friendly Photoprotection

Effective photoprotection is a vital consumer issue. However, there are many concerns regarding the adverse environmental and health impacts associated with current organic and inorganic UV filters. Here, we prepare all-natural eco-friendly UV-absorbing nanoparticles from ethyl cellulose and zein with encapsulated biobased photoprotectants obtainable from plants (quercetin, retinol, and *p*-coumaric acid), which have the potential to satisfy both environmental and health issues in photoprotection. We show the ability for these particles to be easily tuned compositionally, and prepare transparent UV-absorbing coatings from these particles. We then study the retention and incorporation of quercetin, retinol, and *p*-coumaric acid into the ethyl cellulose nanoparticles. These results have significant implications for the development of novel photoprotection technologies and functional nanoparticles.

1 Introduction

Excessive exposure to UV radiation from sunlight can lead to the degradation of foods and packaging materials, as well as multiple adverse health effects such as sunburn, accelerated skin aging, and the vast majority of skin cancers[69,70]. A part of the UV radiation, UVC (100-290 nm), is filtered out completely in the atmosphere but UVB (290-310 nm) and UVA (310-400 nm) radiation reaches our skin[71]. Protection against UV radiation via the use of sunscreens is therefore vital for many consumer products and crucial for human health.

Many current cosmetic sunscreens provide protection across the entire UV spectrum (λ = 290-380 nm) via the use of multiple organic and inorganic UV filters. Despite the effectiveness of synthetic organic and inorganic UV filters in protecting against UV radiation, their use in large quantities has been reported to have significant adverse environmental and health effects. For example, large concentrations of organic UV filters in coastal recreational areas have been strongly linked with accelerated damage to coral reefs[23,72] and marine phytoplankton[73] by promoting viral infections – which has significant implications for the local ecosystem. Inorganic UV filters such as TiO_2 nanoparticles have also been reported as potentially toxic to marine life because they remain photocatalytically active in the environment[74,75]. As for health concerns, inorganic and synthetic organic UV filters have been identified as phototoxic[22,76], potent skin allergens[77], and have been reported to penetrate the skin and act as endocrine disruptors in the bloodstream[19,78].

One method to address the *health* concerns of inorganic and synthetic organic UV filters is to minimize skin contact with the UV filters. Skin contact can be minimized for inorganic UV filters via coating the particles (i.e. with silica/alumina) and for organic UV filters via encapsulation into nanoparticles from materials such as silica[21], gelatin[79], lipids[80], poly-lactide[81], and ethyl cellulose (EC)[22]. The coating of inorganic UV filters and encapsulation of organic UV filters can result in significant reduction of direct skin contact[19,82], skin penetration[19], and reduction in the phototoxicity[21,22]. Furthermore, encapsulation of organic UV filters into nanoparticles also reduces the need for unnecessary chemicals (i.e. surfactants used in formulation), can increase photostability[81], and potentially allows higher loadings in formulations – the amount of organic UV filter in the formulation is no longer limited by its solubility[83]. Despite the advantages of nanoencapsulation, the adverse health effects of the synthetic UV filters cannot be completely eliminated and their environmental impact remains a concern. Thus, the replacement of synthetic UV filters with eco-friendly, natural, biobased photoprotectants – which are potentially safer[84] – and encapsulation into eco-friendly nanoparticles has the potential to satisfy both environmental and health concerns whilst providing effective photoprotection.

There are many known biobased photoprotectants, such as flavonoids (i.e. quercetin and rutin), lignin (i.e. *p*-coumaric acid), and carotenoids (i.e. β-carotene, lutein, lycopene, retinol). Quercetin and rutin are the most extensively studied biobased photoprotectants, and both have even been individually incorporated into solid-lipid nanoparticles (SLNs) for sunscreen applications[79,84,85]. Despite this, there is still a need to develop UV-absorbing nanoparticles with an entirely natural composition which can: i) efficiently encapsulate multiple biobased photoprotectants, ii) provide broadband and uniform UV absorbance, iii) prepare effective UV-protective coatings, and iv) be potentially used for multiple solvent systems e.g. oil and emulsion (SLNs will simply dissolve in oil based formulations), for effective eco-friendly photoprotection.

Here, all-natural UV-absorbing nanoparticles are developed via the encapsulation of multiple biobased photoprotectants together into biobased ethyl cellulose nanoparticles (ECNPs) and biobased zein nanoparticles (ZNPs) using an upscalable technique. As a protein, zein may not be suitable for skincare applications but is potentially very interesting for photoprotection in food packaging materials, and is moreover an interesting material because it absorbs UV light itself primarily due to the presence of xanthophylls and β-carotene[86]. In this work will be shown that the all-natural UV-absorbing ECNPs and ZNPs with encapsulated quercetin, retinol, and coumaric acid can provide effective uniform broadband UV spectrum protection. Then will be focused on the UV-absorbing ECNPs and transparent, flexible coatings with tuneable thicknesses will be prepared, including the photodegradation study of these coatings. Additionally, the retention of the biobased photoprotectants inside the ECNPs and the incorporation of the biobased photoprotectants into the ECNPs is studied.

The findings in this chapter are significant for the development of safer and more environmentally friendly methods of photoprotection, and have important implications for the more general fields of UV protective coatings and functional nanoparticles.

2 Theory

2.1 Encapsulation mechanism

In the previous chapter the anti-solvent precipitation technique and its most important parameters have already been discussed. The theory of this chapter will focus on the mechanism of encapsulation during such anti-solvent precipitation methods and some theory about plant based photoprotectants will be discussed.

The production of nanoparticles using anti-solvent precipitation is often divided into two categories: (i) compound particles – particles entirely formed from the active compound itself (Figure 10A)[66]; (ii) composite particles – particles formed from the active component and one or more excipients (Figure 10B-D). These excipients are typically polymers, surfactants or polysaccharides. The compound(s) to be entrapped is/are referred to as the "active" material, whereas the material that forms the surrounding particle matrix is usually referred to as the "encapsulant" or "carrier" material. Depending on physicochemical characteristics of the active material and encapsulant, and the preparation conditions, the nanoparticles may have different morphologies[87].

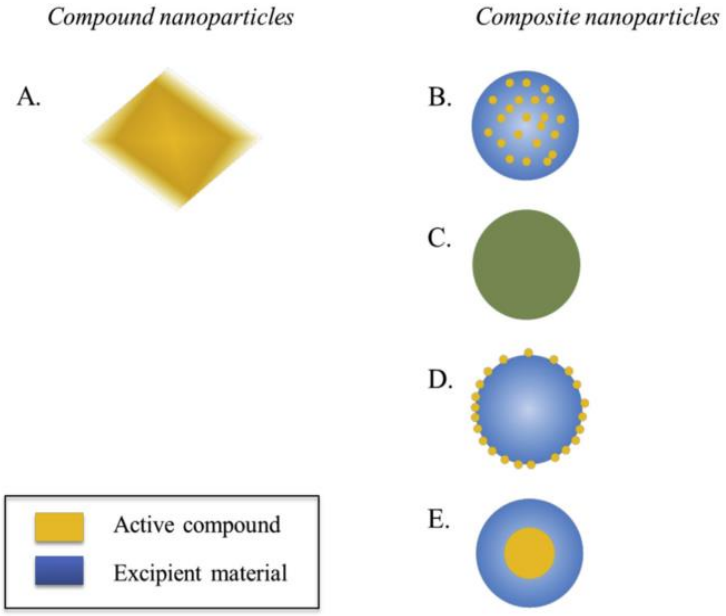

Figure 10: Cross sections of different nanoparticle structures. The nanoparticles can be composed of the pure compound of interest (A), i.e. compound nanoparticles; or contain an excipient matrix material, in which the active compound is enclosed as a colloidal (B) or molecular (C) dispersion, or at which surface it is adsorbed (D). A fifth possible structure is a core which consists of the compound of interest, which is protected by a surface layer composed of the excipient material (E). The latter structures (B-E) are typical examples of composite nanoparticles[7].

Compound nanoparticles made from pure active compound (which are commonly crystalline or amorphous solids) may show a broad range of morphologies, such as needles, cubes, ellipsoids and spheres. The dissolution rate of the drug can be affected by the physical state of the active compound and must therefore be precisely controlled during the formation of compound particles. Amorphous or metastable forms have higher internal energy and greater molecular mobility, therefore these forms tend to dissolve faster than crystalline forms[51]. Likewise, different polymorphic forms typically have different dissolution rates, so to ensure that the required polymorphic form is produced the preparation conditions should be controlled.

Composite nanoparticles prepared by an anti-solvent precipitation method are often spherical, but their internal structures may vary greatly (Figure 10): molecular composites – molecular dispersion of active compound throughout polymer matrix; dispersion composites – colloidal dispersion of active compound throughout polymer matrix; core-shell – active core surrounded by polymer shell (or polymer core surrounded by active shell). The method of entrapping active compounds in composite nanoparticles made up of polymers was developed a couple of decades ago. Composite particles are usually formed by simultaneous precipitation of the core (i.e. the active ingredient likely to be encapsulated) and coating material (i.e. the biopolymer material)[60], the active ingredient must therefore have the same properties (in terms of solubility in the anti-solvent/solvent system) as the coating material. The polymers have several functions such as providing stability to the particles and bioactive compounds in a complex matrix, and upon processing, but at the same time also enhance the control over compound release. The bioactive compounds interact physically or bind chemically (covalent bonding) to the excipient material in these particles. Upon molecular encapsulation (Figure 10), the form of the encapsulated active compound is in general not crystalline because crystallization is inhibited by the polymer matrix[88]. The form of the active ingredient in dispersion composites and core-shell structures may be liquid, amorphous or crystalline depending on its properties.

2.2 Active material - photoprotection by plant extracts

Composite nanoparticles can be functionalized by the encapsulation of an active drug compound, where the properties of the active drug compound often determines the performance of the nanoparticle. By the encapsulation of photoprotectant material, composite nanoparticles can be used for photoprotection.

In recent years the great importance of reducing concentrations of chemical UV filters in sunscreens by using natural products for their higher tolerability and for their negligible environmental impact is addressed[89]. The development of sunscreen formulations containing plant extracts is extensively being explored. Plant extracts are able to prevent UV-induced skin photodamage, including the risk of skin cancer, because they contain polyphenols which resemble in chemical structure to organic UV filters. Polyphenols are very sensitive to environmental factors, such as heat and light, and generally show low water solubility in their free form, affecting its bioavailability. The encapsulation of polyphenols into nanoparticles and nano emulsions have been investigated in order to improve their stability and preserve the bioactivity of the compounds[90].

Polyphenols consist out of one or several aromatic rings bearing one or more hydroxyl functionalities, usually conjugated to sugars or organic acids[91]. One of the two main categories of polyphenols are flavonoids. These are low-molecular-weight compounds; the basic structure corresponds to two benzene rings (A and B) linked through a heterocyclic pyran or pyrone (with double bond) ring (C) in the middle[92] (Figure 11).

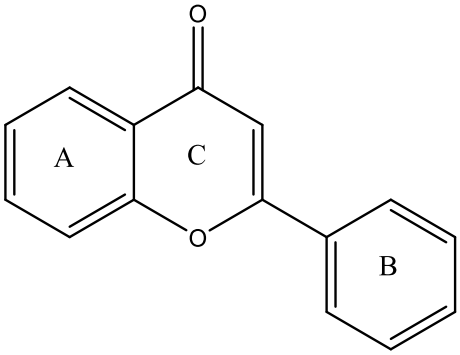

Figure 11: general molecular structure of a polyphenol.

As expected for aromatic compounds, flavonoids absorb UV radiation from 250 to 400 nm. Their photo physical and photochemical transformations involves $\pi\pi^*$ excited states. They can transfer or accept energy from substrates in the environment, react from $\pi\pi^*$ excited states, or deactivate ROS produced in plants after intensive UV exposure[93,94].

One of the most common and effective UV protective flavonoids is quercetin. Figure 12 depicts the molecular structure of quercetin. This flavonoid is able to deliver photoprotection due to the direct absorption of the UV radiation, and prevention of ROS production and direct DNA damage. The UV energy absorbed by quercetin may be dissipated as heat, light or through decomposition[94].

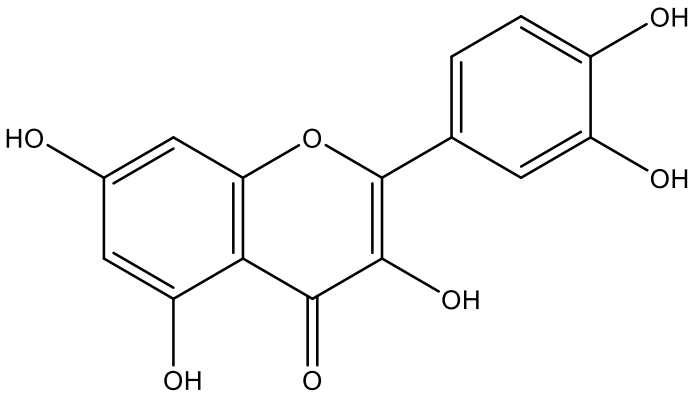

Figure 12: molecular structure of quercetin.

Nonflavonoid polyphenols consist of a heterogeneous group including phenolic acids, hydroxycinnamates, stilbenes, lignans, and tannins.

Phenolic acids are simple molecules such as caffeic acid, and coumaric acid. Phenolic acids form a diverse group that includes the widely distributed hydroxybenzoic and hydroxycinnamic acids. Hydroxycinnamic acid compounds (p-coumaric, caffeic acid, ferulic acid) occur most frequently as simple esters with hydroxy carboxylic acids or glucose, while the hydroxybenzoic acid compounds (p-hydroxybenzoic, gallic acid, ellagic acid) are present mainly in the form of glucosides[89].

Coumaric acid (chemical structure Figure 13) is a suitable polyphenol for the incorporation into nanoparticles due to its hydrophobic characteristic. Its adsorption peak around 310-320 nm allows the protection of UV light in the UV-B region.

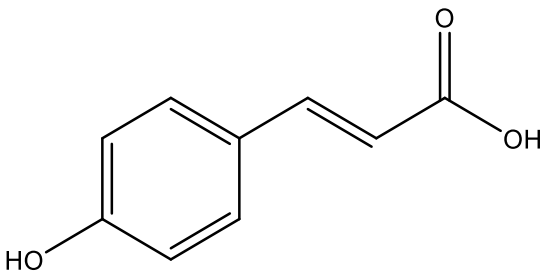

Figure 13: molecular structure of p-coumaric acid.

Another class of UV absorbing plants extracts are carotenoids. Carotenoids, such as b-carotene, lutein and lycopene are natural lipophilic pigments which are extensively found in nature and have several biological functions and health benefits[84]. Carotenoids are extremely hydrophobic molecules with little or no solubility in water and have a strong tendency to aggregate in aqueous solutions. The structural details, such as shape, size, and hydrophobicity, of carotenoids may define the interactions of this molecule with its surroundings. Since carotenoids are unstable at high temperatures, in the presence of light and oxygen, their incorporation into micro- and nanostructures is an alternative method to increase their stability and preserve their antioxidant and provitamin A activities in many environmental conditions[95].

Retinol (chemical structure Figure 14) and its derivatives are extensively used in the pharmaceutical and cosmetic area. Retinol (vitamin A) is an interesting carotenoid to study as a replacement for traditional UV filters in sunscreens because retinoids are recognized as being important for modern therapy of dermatological treatment of wrinkled skin[96].

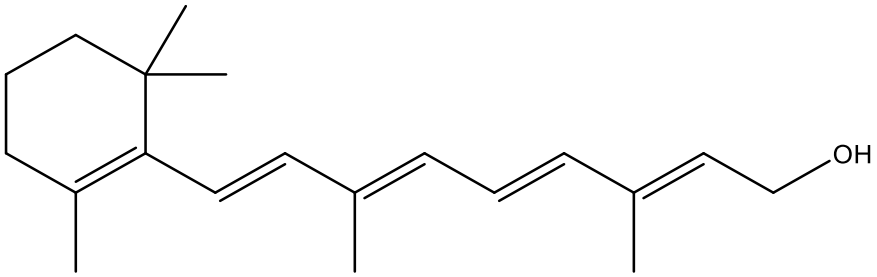

Figure 14: molecular structure of retinol.

Retinol strongly absorbs ultraviolet (UV) radiation between 300 and 350 nm, with a maximum at 325 nm[97]. The beneficial effects of carotenoids, in UV light protection, have to do with their capacity to act as quenchers of photosensitization products and also as inhibitors of free radical reactions.

3 Experimental details

3.1 Materials

Ethyl cellulose (EC) degree of substitution 2.1-2.6 (100 cP, lot number MKBT0521V), Quercetin (≥95%, solubility in water 60 mg/L at 16°C (PubChem database)), retinol (synthetic ≥95%, solubility in water 0.67 mg/L at 25°C (PubChem database)), *p*-coumaric acid (98%, solubility in water 1020 mg/L at 24°C (Drugbank database), were all purchased from Sigma Aldrich.

Ethanol (100%) was purchased from Interchema and pure water was used from a Millipore system

3.2 Methods

Synthesis of ECNPs/ZNPs with UV filters encapsulated

The three natural and biodegradable UV filters were encapsulated into ECNPs and ZNPs (<100 nm) via a simple, upscalable, surfactant-free "antisolvent precipitation" technique from literature[22,98]. Encapsulation of the filters during the anti-solvent procedure occurs due to the co-precipitation of the hydrophobic UV filters together with the hydrophobic ethyl cellulose or zein. In this "antisolvent precipitation" procedure, EC (for ECNPs) or zein (for ZNPs) and the UV filters are dissolved together in ethanol at the desired concentrations (for ECNPs) or an ethanol/water mixture (80 (v/v)% EtOH) (for ZNPs). Subsequently, this solution is poured into the anti-solvent water (150 mL, pH 5-6) under fast magnetic stirring, resulting in the spontaneous formation of ECNPs/ZNPs with encapsulated UV filters. This procedure is schematically depicted in Figure 15, and differs from Figure 3 (in chapter 1) in the co-dissolvement of the natural UV filters together with EC in ethanol.

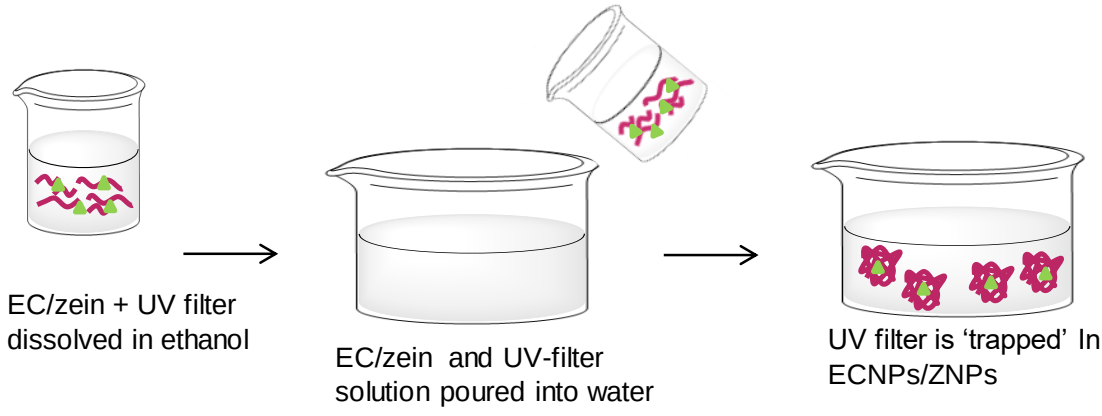

Figure 15: schematically depicted co precipitation of UV filters together with EC/zein.

Rotary evaporation removed ethanol and some water resulting in 5.35 g L^{-1} and 7.0 g L^{-1} stable aqueous colloidal dispersion of ECNPs and ZNPs respectively. The resultant ECNP dispersions were passed through a 1.2 µm filter to remove any large aggregates formed during the antisolvent precipitation. The ZNPs were filtered with filter paper (pore size 11 µm) in order to avoid precipitation of the protein particles onto to the filter. During the experiments the

concentration of EC and zein was kept constant but the amount of natural UV filter was varied. The varying amounts of natural UV filter are expressed in wt.%. 5 wt.% means that 5% of the total added amount of EC/zein is added as UV filter (e.g. 5 wt.% is 1 g of EC + 0.05 g of UV filter).

Preparation of UV-protective coatings

In order to prepare UV coatings, a concentrated dispersion (30 g L^{-1}) of the ECNPs was spin coated onto plasma-cleaned, circular glass microscope cover slips (22 mm) at 1800 rpm for 1 minute (spin-coater: SCS P6700). Additional layers were spin coated onto the original coating layer to increase the coating thickness.

3.3 Characterization

Spectroscopic characterization

UV-VIS spectra of the dispersions were obtained by the use of a HP 8452a spectrophotometer. Dispersions (5.35 x 10^{-3} g L^{-1}) were a diluted a hundred of times with miliQ water (pH 5-6) for ECNPs and with acidified water (pH 3.5) for ZNPs before recording the spectra.

Size characterization

Size characterization of ECNPs and ZNPs was done with DLS measurements (Malvern Zetasizer Nano ZS, particle size distributions were obtained by using a Contin algorithm) and SEM imaging (FEI XL30FEG). The samples were diluted with miliQ water (pH 5-6) for ECNPs and with acidified water (pH 3.5) for ZNPs. To prevent charging of the particles during SEM imaging, the particles were sputter coated using platinum.

Zeta potential measurements

Zeta potentials of the particles were determined by electrophoretic mobility using a Malvern Zetasizer Nano ZS, operating at 148 V at equal particle concentrations, equal dilutions, and in the presence of a background salt (10 mM NaCl). The pH was also kept constant (that of milliQ water, pH 5-6 for ECNPs and acidic water, pH 3.5 for ZNPs). Each sample was analysed in triplicate, at a temperature of 20 ^{o}C one day after preparation of the ECNPs dispersion.

Encapsulation efficiency

The amount of loaded quercetin was determined by drying the dispersion at elevated temperature (80 ^{o}C), redissolving a weighted amount of these dried ECNPs and UV filter in ethanol, measuring the absorbance and comparing with a calibration curve of known concentrations.

Photo stability studies of natural UV filters in ECNPs

The photo stability of the natural UV filters in ECNPs was investigated by subjecting coatings, with spin coated dispersions of ECNPs with UV filters, to irradiation by a 75 W Xenon lamp at a distance of 15 cm (a flux of 3 mW cm^{-2} between 300 and 400 nm). The absorbance was measured hourly for four hours. The total UV dose was thus 432 kJ m^{-2}; equivalent to 2 hours 24 minutes of summer sunlight in Nice at noon[99].

Fourier Transform infrared (FTIR) spectroscopy

The FTIR spectra of the samples were obtained on a Perkin-Elmer SpectrumTwo UATR FTIR spectrophotometer. Samples in the solid state were measured in KBr matrix. All FTIR spectra were collected at a spectral resolution of 4 cm^{-1}, with 32 co-added scans over the range from 4000 to 450 cm^{-1}. A background scan of clean KBr-Diamond crystal was acquired before scanning the samples. The Perkin-Elmer software was used to perform baseline corrections, normalization and peak integration of the spectra. ECNP dispersions with 10 wt.% encapsulated UV-filter were dried at 80 ^{o}C in order to obtain the nanoparticles in a solid form.

Retention

10 ml of 5.35 x 10^{-3} g L^{-1} ECNPs with individual encapsulated UV filter were placed in a dialysis membrane bag with a molecular cut-off of 40 kDa, tied and placed into 300 ml of water. The entire system was kept at room temperature with continuous magnetic stirring. Retention was determined by measuring the absorbance of a sample taken from the dialysis tubing after 24h, 48h, and 72h in separate experiments to avoid inaccuracy through measurement.

4 Results and Discussion

4.1 Individual encapsulation: preparation

In a first stage, the individual encapsulation of the three plants extracts (with UV absorbing properties) coumaric acid, retinol and quercetin into ECNPs was studied. These three UV absorbing compounds found in plant extracts where chosen because they each absorb UV light of different wavelengths covering the whole UVA and UVB spectrum, and have similar soluble properties (hydrophobic) as EC and zein.

Studying the individual encapsulation of these UV filters into ECNPs is crucial in giving a better understanding of how to prepare effective all-natural broadband UV-absorbing NPs.

ECNPs with sizes of around 70 nm in diameter were chosen to use for the encapsulation of the UV-filters because these are the largest ECNPs that can be prepared with a very high yield (>80%) (Chapter 1, Figure 9) and limited scattering.

In order to study the encapsulation, a series of aqueous ECNP dispersions for each biobased UV filter was prepared. The three series of dispersions contain equal amounts of EC but varying amounts of the natural UV filters (0, 5, 10, 20, 35 and 50 wt.%), which are prepared by dissolving the UV filters together with EC in ethanol before undergoing the anti-solvent precipitation. The three series are depicted in Figure 16, where it can been observed that when the amount of added UV filter increases the colour of the dispersion becomes more intense, which may indicate that more UV filter is encapsulated. Apparently, the UV-filters absorption spectrum extends into the blue part of the visible spectrum.

(a)

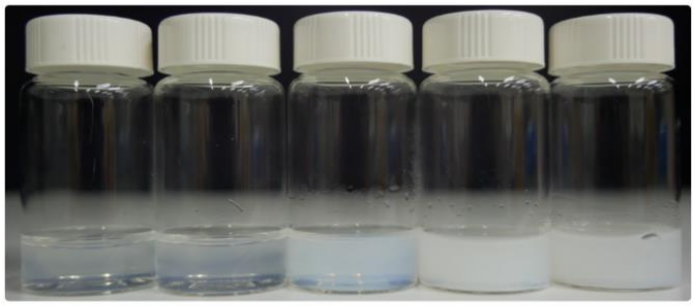

(b)

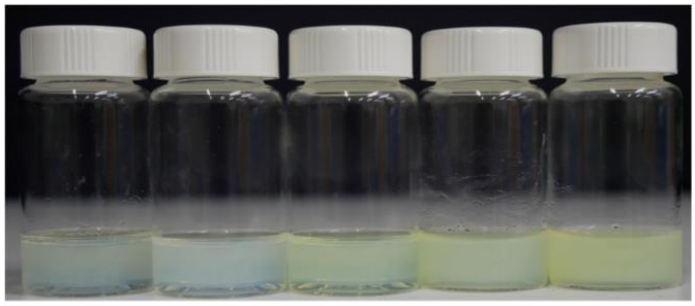

(c)

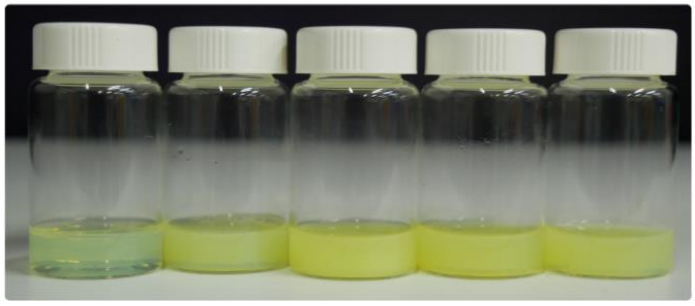

Figure 16: photo of the three series of dispersions with 5, 10, 20, 35 and 50 wt.% (from left to right) encapsulated UV filters (a) coumaric acid (b) retinol (c) quercetin.

4.2 Individual encapsulation: characterization

The ratio of polymer to active compound, in composite particles, is crucial since it alters particle formation, stability and loading capacity[60]. Different properties (size, zeta potential, absorbance, and maximum particle loading) of the ECNPs containing UV filter were therefore studied.

Size

Size characterization of the ECNPs upon loading of UV-filter was studied because maintaining small particle sizes is desirable when the particles are applied as coatings in order to keep transparency and thus remain appealing for cosmetic applications.

Figure 17 depicts the average sizes of the ECNPs particles, when individually encapsulated with one of the UV filters, as a function of their absorbance. DLS spectra can be found in the appendix (Figure B1-B3). The size is plotted against the absorbance and not against the wt.% encapsulated material because the particles of a maximum particle loading around 15 wt.% and above these percentages the amount of encapsulated material cannot always be determined.

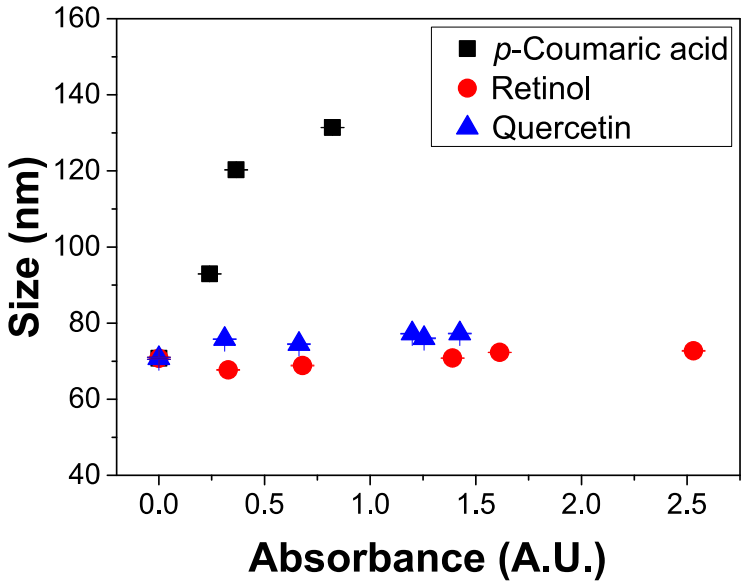

Figure 17: average particle size measurements, as determined by DLS, as a function of UV filter loading for the three series of ECNPs in which varying amounts of coumaric acid, retinol and quercetin are individually encapsulated.

The average size of the ECNPs was found to remain constant (70-75 nm) upon increasing loadings of quercetin and retinol and the DLS spectra show narrow size distributions (appendix B). However, the size of the ECNPs encapsulated with coumaric acid increased significantly upon the addition of greater amounts of coumaric acid (70-140 nm). Another observation for the increase in particle size for loading upon *p*-coumaric acid is the scattering of the particles which can be observed in Figure 16. By comparing the most right vials of each series, in Figure 16, can be seen that most right vials for the series of *p*-coumaric acid start to scatter light whereas the series of dispersions for quercetin and retinol stay more transparent.

This increase in particle size (according to the increase in particle size) has also been reported by Thünemann *et al.*[100] and Kim *et al.*[101] for the loading of retinoic acid into polyethylenimine nanoparticles and retinol into chitosan nanoparticles respectively, where the increase in particle size is attributed to ion complex formation.

Moreover, when amounts of coumaric acid greater than 20 wt.% were added, a bimodal distribution of ECNPs was observed. Figure B1 depicts the DLS spectra of the ECNPs when 35 and 50 wt.% of coumaric acid is encapsulated, and larger micron sized particles can be observed. This larger set of particles is likely pure coumaric acid or coumaric acid with some EC at the interface. This was verified by performing the anti-solvent precipitation with only pure coumaric acid (and no EC). Figure 18 shows the DLS spectrum of the formed dispersion where the similarly micron sized particles can be observed. This phenomenon has previously been reported for the encapsulation of large amounts of other organic molecules into ECNPs.

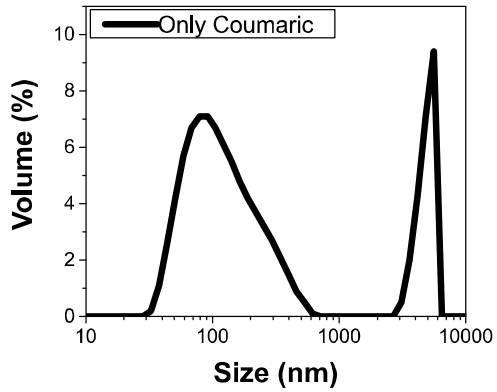

Figure 18. volume weighted size distributions as measured by DLS, of coumaric acid particles which were formed when the anti-solvent precipitation method was only performed with pure coumaric acid.

Polydispersity index (PDI) values provide an indication of the size distribution of the particles present in suspension. PDI values smaller than 0.2 are considered ideal, while PDI values higher than 0.5 are indicative of a very broad size distribution[102]. The PDI values as measured by DLS of the three series of dispersions are summarized in Table 1. The PDI values of ECNPs with quercetin and retinol did not significantly change upon addition of greater amounts and are between 0.124 and 0.160. For the addition of 20 wt.% coumaric acid in ECNPs a PDI of 0.230 was found.

Table 1: PDI values of the three series of dispersions as measured by DLS

Sample	Size average (nm)	Error (nm)	PDI
Quercetin 5%	76	0.05	0.128
Quercetin 10%	75	0.10	0.131
Quercetin 20%	76	0.10	0.130
Quercetin 35%	77	0.10	0.124
Quercetin 50%	77	0.10	0.160
Retinol 5%	68	0.10	0.140
Retinol 10%	69	0.10	0.138
Retinol 20%	71	0.05	0.151
Retinol 35%	72	0.05	0.154
Retinol 50%	73	0.10	0.161
Coumaric acid 5%	93	0.05	0.105
Coumaric acid 10%	120	0.10	0.110
Coumaric acid 20%	131	0.05	0.230
No UV-filter added	71	0.27	0.158

Thus, the encapsulation of greater amounts (> 10 wt.%) of retinol and quercetin are more favourable than coumaric acid with respect to maintaining smaller particle sizes and polydispersity of the dispersion.

Zeta potential

Zeta potential measurements were performed to investigate two factors associated with the incorporation of UV filters into ECNPs: i) whether the dispersion was made more/less colloidally stable (and therefore prone to particle aggregation) by the encapsulation of UV filters, where a decrease in negative values or increase in positive values indicates improved stability and ii) whether the UV filters exist surface bound, inside the ECNPs, or both upon encapsulation.

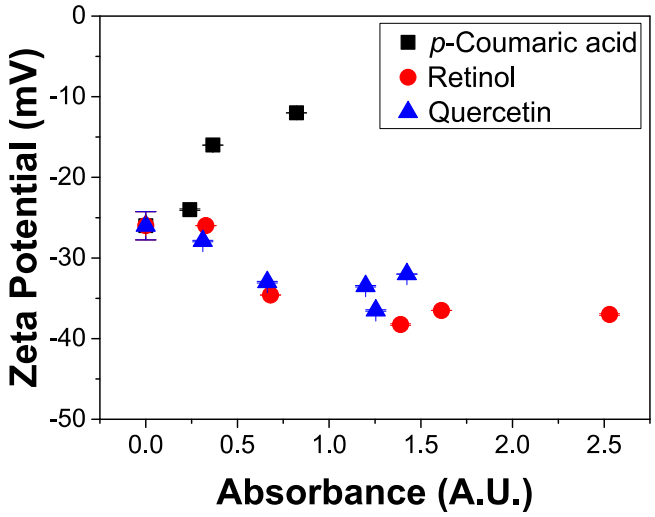

Figure 19: zeta potential as a function of UV filter loading for the three series of ECNPs in which varying amounts of coumaric acid, retinol and quercetin are individually encapsulated.

With respect to the former point, Figure 19 shows that the zeta potential of the ECNPs was affected very little upon increasing amounts of encapsulated quercetin or retinol and has therefore no limitation to the dispersion stability. However, when the ECNPs were loaded with large amounts (>10 wt.%) of coumaric acid the absolute zeta potential decreased considerably upon greater amounts of encapsulated UV filter, leading to less stable dispersions

With respect to the second point, it is desirable that UV filters are *less* surface bound because the intended application is for cosmetic UV protection – therefore skin contact is minimized. A minimal (negative) decrease in zeta potential was observed for loadings of quercetin and retinol, which implies that the a small alteration of the surface occurs when loaded within ECNPs. However, the molecules are both neutral (at the pH of the dispersion) and therefore may be present on the surface without contributing towards the zeta potential. For coumaric acid can be seen that the absolute zeta potential decreases with increasing loading. This is surprising because coumaric acid has a negative charge and one may expect a higher loading of coumaric acid on the surface to result in a greater absolute zeta potential.

Absorbance

Absorbance spectra of the three series of dispersions were recorded to study the efficiency of the encapsulation of natural UV filters into ECNPs.

Figure 20 (a,b,c) shows the absorbance curves of the dispersion series of ECNPs with UV filters encapsulated. For each UV filter a general trend can be observed – the absorbance increases when larger amounts of UV filter are dissolved in the initial ethanol solution and encapsulation is therefore efficient. However, the extent of loading varied between UV filters. For example, up to 50 wt.% retinol could be encapsulated efficiently, whereas only up to 20 wt.% for quercetin and coumaric acid. For quercetin the absorbance begins to level off for additions of more than 20 wt.% (Figure 20c). This implies that the ECNPs are saturated with the maximum possible loading of quercetin and the excess quercetin in the reaction that is not encapsulated must therefore be filtered out after the antisolvent precipitation. While for the loading of ECNPs with coumaric acid, addition of more than 20 wt.% led to the formation of a separate set of micron-sized particles as earlier discussed within the size characterization. This is also the reason why Figure 20a is without an absorbance curve for 35 and 50 wt.% coumaric acid.

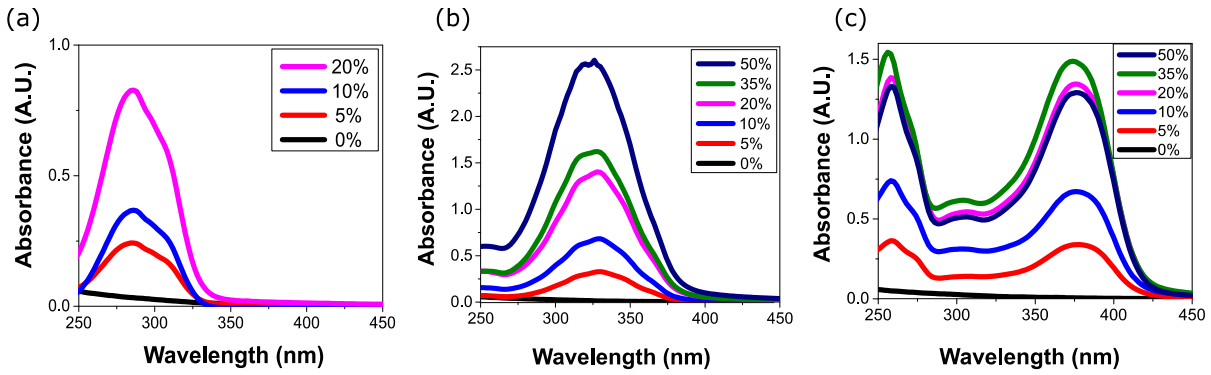

Figure 20: absorption measurements at a concentration of 6.1 x 10 $^{-5}$ g L^{-1} for the three series of ECNPs in which varying amounts of coumaric acid (a), retinol (b) and quercetin (c) are individually encapsulated.

In terms of efficient encapsulation can be concluded that retinol encapsulates the most efficient without having a maximum particle loading or the formation of micron particles of only retinol.

Maximum particle loading

The maximum particle loading was further studied because insight into the efficiency of the encapsulation can avoid the addition of excess (not encapsulated) UV filter.

In Figure 20c can be seen that the absorbance appears to level off after the addition of greater amounts of quercetin than ~20wt.%, indicating that the ECNPs become saturated with quercetin at around this point. Insight into the efficiency of the encapsulation was obtained by determining the amount of loaded quercetin inside the ECNPs for the prepared series.

Figure 21 depicts the amounts of initially added quercetin as a function of the actual amount of quercetin found in the ECNPs. The efficiency was close to 100% for the encapsulation of 5, 10, and 20 wt.% quercetin (where a 100% encapsulation efficiency of 20 wt.% quercetin added would result in particles in which a total of 100*20/120 =16 wt.% is UV filter), but lowered considerably thereafter. The maximum loading plateaued at approximately 10-14 wt.%. It was not possible to acquire a similar insight into the encapsulation of coumaric acid and retinol

because they lost a considerable amount of their absorbance during the drying at elevated temperature (80°C). Carotenoids such as retinol are known to be unstable when exposed to air thus not in solution form[95], whilst coumaric acid is known to lose absorbance due to a cis/trans isomerization[103].

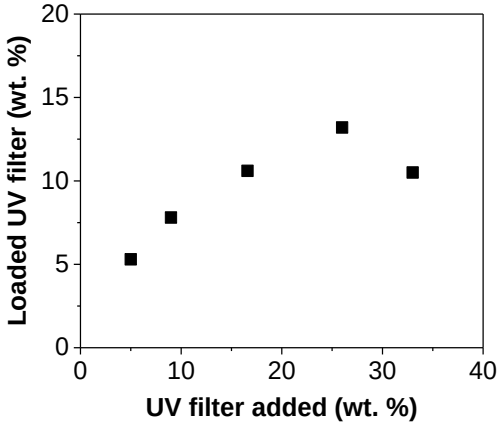

Figure 21: Amount of quercetin loaded into the ECNPs as a function of the amount added. The prepared dispersion refer to the addition of 5, 10, 20, 35, and 50 wt.% of quercetin (i.e. the addition of 50 wt.% means 1 g EC + 0.5 g of quercetin). The values are therefore translated as 5, 9, 17, 26, 33 wt.% of the total wt.% of the entire composite particle (50 wt.% added is therefore 100[0.5 g / 1 g + 0.5 g] = 33%).*

FTIR analysis

FTIR analysis is one of the important tools for the quick and efficient identification of encapsulated chemical molecules. In Figure 22 we show the FTIR spectra from the pure materials EC, quercetin, retinol and *p*-coumaric acid, as well as ECNPs with the three biobased photoprotectants encapsulated individually at 10 wt.%. FTIR spectra of the pure compounds can be found in appendix C.

The spectra of all mixtures seemed to be mainly a summation of pure quercetin/retinol/*p*-coumaric acid and EC spectra. The major characteristic peaks of EC corresponding to –C–O–C– stretching vibration (1053 cm^{-1}); C–H stretching bands (2876 cm^{-1} and 2973 cm^{-1}); C–H bending (1370 cm^{-1}) [104] were present as prominent peaks in all FTIR spectra of the ECNPs individually encapsulated with the three UV filters.

However, between 1600 and 1700 cm^{-1} the EC showed no characteristic peaks, meaning that the characteristic peaks from each photoprotectant could be observed.

The spectrum of ECNPs with quercetin encapsulated shows two characteristic peaks between 1600 and 1700 cm^{-1}, which are also observed in the spectrum of the pure compound. The peak at 1599 cm^{-1} corresponds to conjugated aromatic C=C stretching and the peak at 1654 cm^{-1} to -CO stretching[105].

In the spectrum of the ECNPs with retinol encapsulated the characteristic peaks of retinol at 1727 cm^{-1} can be observed, which corresponds to C=C conjugated aromatic stretching[105]. However, this peak is broader than compared to the pure retinol.

In the spectrum of ECNPs with *p*-coumaric acid encapsulated the main characteristic peaks of *p*-coumaric acid in the region 1500 to 1700 cm^{-1} can be observed. The band at 1606 cm^{-1} is due to C=C aromatic stretching, whereas the bands at 1515 cm^{-1} is assigned to C–H bending

vibrations from the aromatic ring. The band at 1635 cm^{-1} is assigned to C=C stretching vibrations of the aliphatic group and the band at 1669 cm^{-1} is typical for the C=O stretching of carboxylic acids[106]. The peak ratio between these characteristic peaks, however, differs from the ratio observed in the spectrum of the pure sample.

The fact that no peaks disappear and no new peaks are observed (in the region 1600 to 1700 cm^{-1}) means that the photoprotectants do not change in chemical structure upon encapsulation, which indicates physical encapsulation into the ECNPs (as opposed to covalent bonds forming between the EC and photoprotectant). However, the slight alteration in peak ratio/broadening of the peaks in the spectra of the ECNPs encapsulated with retinol and *p*-coumaric acid may point at interactions between these active materials and EC used in formation of colloidal particles[18].

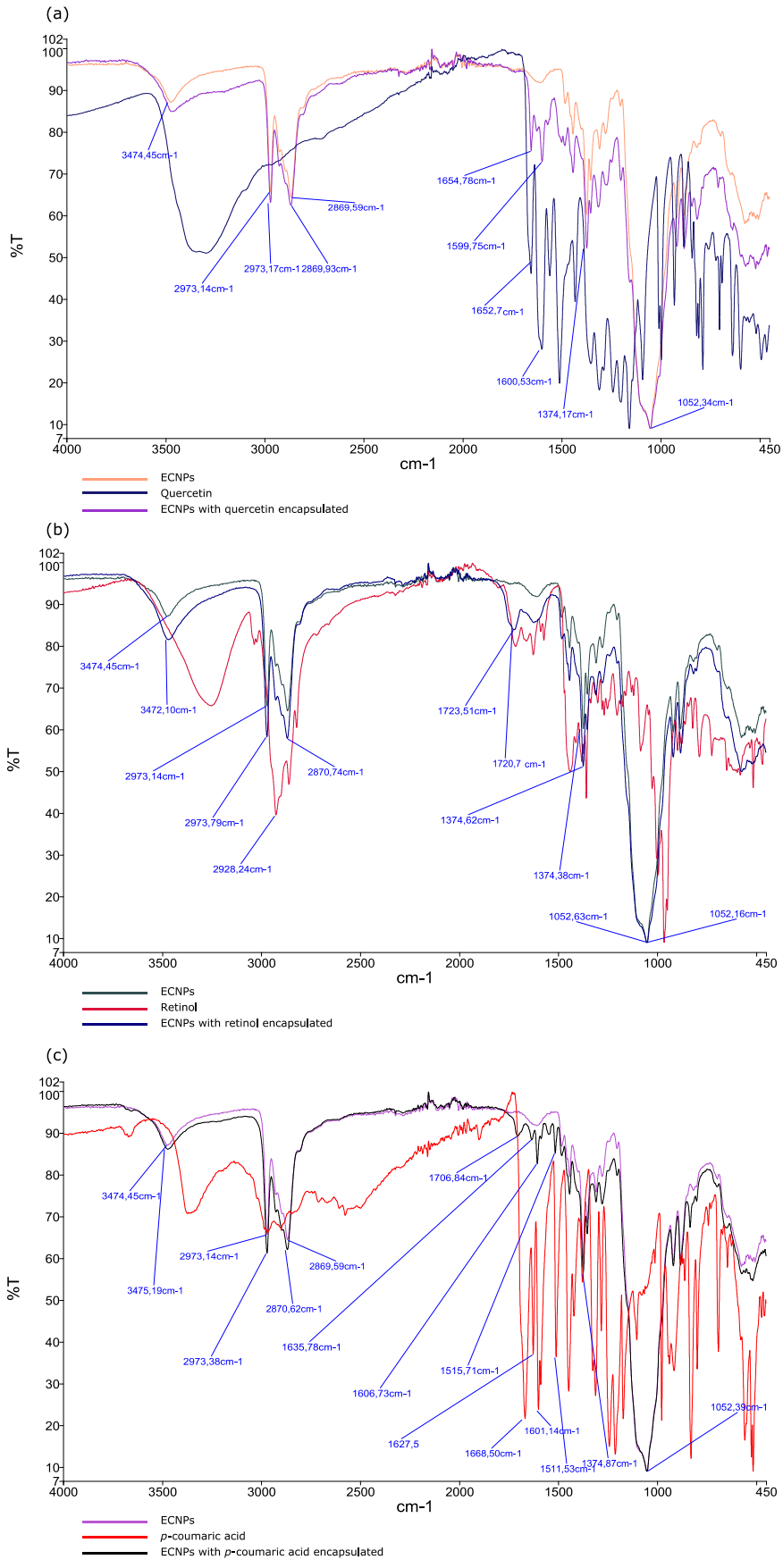

Figure 22: FTIR analysis of ECNPs, pure active material and ECNPs individually encapsulated with each UV filter (a) quercetin, (b) retinol and (c) p-coumaric acid.

Retention of the UV filters within ECNPs

Retention of the UV filters within the ECNPs is investigated because leaching of the UV filters could decrease UV protection and make the particles less useful.

FTIR data indicated at physical encapsulation of the UV filters into the ECNPs. Physical encapsulation of UV filters into nanoparticles is known to be prone to leaching, since the molecules are not covalently bound to the nanoparticle[107,108]. Although covalent encapsulation of organic UV filters is possible and has been shown to dramatically increase retention[107], covalent encapsulation is unrealistic for commercial use because these modified molecules need to be legislatively reapproved. For example, in the U.S. only 3 new UV filters (zinc oxide, avobenzone, and ecamsule) have been approved since 1978[109].

For these retention experiments the absorbance of 10 mL of the UV absorbing nanoparticles in dialysis tubing was measured at time intervals (24h, 48h, 72h) when sitting in a very large body of water (300 mL). It must be noted that these results represent the retention in the particles when in large bodies of water, as opposed to smaller volumes of water, like in formulations. The retention in the ECNPs in formulations will likely be far greater, allowing for a longer shelf life of the formulations. Also, these measurements do not simulate the retention behaviour of these particles when applied on skin or food packaging materials as a coating.

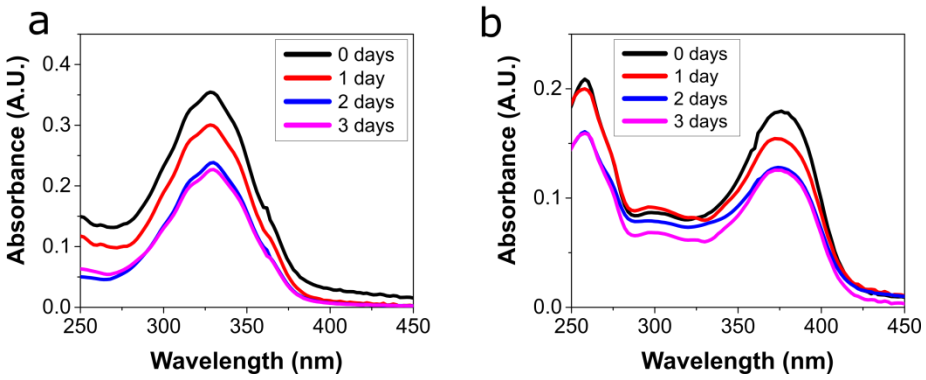

Figure 23: absorption spectra showing the release of retinol (a) and quercetin (b).

Table 2: Percentage of Biobased UV Filters Retained in the ECNPs as a Function of Time

	Retention (%)		
Sample	**24h**	**48h**	**72h**
Quercetin	86	71	70
Retinol	85	67	64

Figure 23 depicts the measured absorbance spectra of the samples at the set time intervals (24h, 48h, 72h, 96h), which are converted to retention percentages and summarized in Table 2. These results show that the biobased photoprotectants quercetin and retinol were effectively retained inside the ECNPs with 64-70% after 72 hours . These values are similar to synthetic UV filters physically encapsulated into nanoparticles developed for sunscreen applications[21,110,111]. The retention of coumaric acid could not be measured accurately via our spectrophotometric method because the molecule is prone to cis-trans isomerisation which changes the absorbance[103].

These biobased UV-absorbing nanoparticles therefore demonstrate effective retention values, with the additional advantage that if these biobased photoprotectants are released into the environment they are not reported to have such detrimental environmental impacts as their synthetic counterparts to i.e. coral reefs.

4.3 Individual encapsulation into ZNPs

Zein is frequently used as a carrier for water active ingredients in food applications because of its food grade properties. The encapsulation of the natural UV filters in zein nanoparticles was briefly investigated, not only for its above named properties but also to see whether the encapsulation of natural UV filters is applicable for other biopolymer material. Zein is also an interesting material because it absorbs UV light itself.

In a first stage zein particles with similar sizes as the ECNPs (70 nm) were prepared. The same anti-solvent precipitation was used, but with a water/ethanol mixture as the solvent. The control of particle sizes for zein nanoparticles is also determined by the initially amount of zein added to the solvent[63].

Zein concentrations were varied to find a particle size which corresponds to the size of the used ECNPs. A concentration of 7.0 g L^{-1} zein in a water/ethanol mixture resulted in the formation of ZNP with an average size of 75 nm and a PDI of 0.110.

In a second stage, dispersions with zein particles of this size and individually encapsulated UV filters at wt.% of 5 and 10 were prepared. As the encapsulation of natural UV filter by zein particles is not the (main) subject of this study only the absorbance of the dispersions was measured and is depicted in Figure 24. An advantage of zein as carrier for natural UV filters is its significant UV absorbance between 250 and 300 nm. The encapsulation follows the same trend as observed for the ECNPs- the absorbance increases when larger amounts of UV filter are dissolved in the initial ethanol solution and encapsulation is therefore efficient. The absorbance for ZNPs with coumaric acid is significantly higher than for retinol and quercetin.

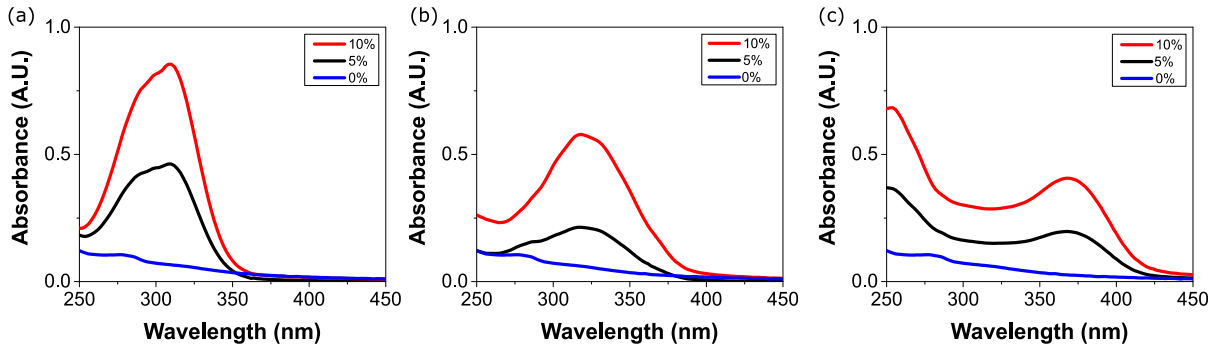

Figure 24: absorption measurements at a concentration of 6.1 x 10 $^{-5}$ g L^{-1} for the three series ZNPs in which varying amounts of coumaric acid (a), retinol (b) and quercetin (c) are individually encapsulated.

4.4 Broadband UV protection: multiple encapsulation

Experimental results in the previous part have shown that the three natural UV filters can individually be encapsulated in ECNPs and ZNPs, where the amount of added UV filter determines its encapsulation efficiency.

Each UV filter covers a different region of the UV spectrum. Multiple encapsulation can therefore lead to coverage of the entire UV spectrum. Nanoparticles which can deliver broad band UV protection are desirable because it will simplify the formulation process.

4.4.1 Broadband ECNPs

First was the multiple encapsulation studied for ECNPs. By using the same anti-solvent co-precipitation as with the individual filters but now dissolving the three filters together, all-natural ECNPs were prepared. The prepared dispersion is depicted in Figure 25 (right vial), with encapsulated quercetin, coumaric acid an retinol in a ratio of 7:1.5:1.5 and a total of 10 wt.%. To show the difference between ECNPs with and without UV filters encapsulated, a dispersion of empty ECNPs is also shown (left vial).

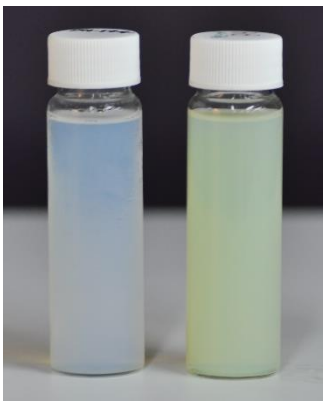

Figure 25: photo of the ECNP dispersion without (left) and with (right) encapsulated UV filters.

Size and stability characterization

The prepared ECNPs with encapsulated UV filters were roughly spherical and had an average particle size of 70 nm and a PDI of 0.101, as seen by DLS measurements (appendix) and SEM imaging (Figure 26). A zeta potential of - 25 mV (at the pH of milliQ water, pH=5-6) was measured and the dispersion was colloidally stable for long periods of time.

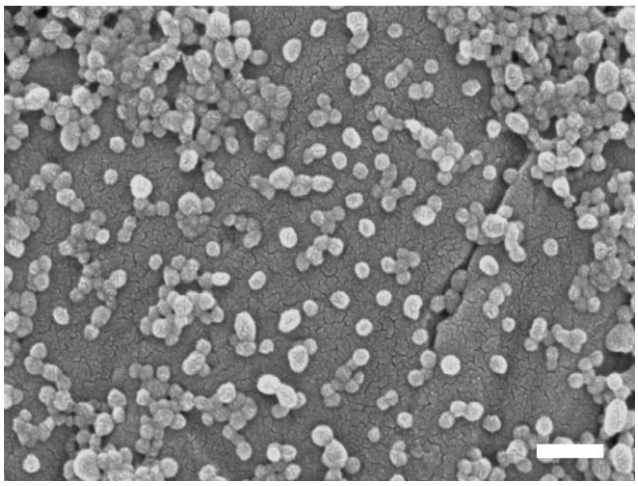

Figure 26: SEM image of ECNPs with all three UV filters encapsulated (scale bar 200 nm)

Absorbance

The amount of UV filter encapsulated could be simply tuned by varying the ratio of each UV filter initially dissolved in the ethanol solution before undergoing the antisolvent precipitation. The actual amount of encapsulated UV filter also determines the quantity of UV absorption in a certain region. A 1:1:1 ratio of the three UV filters (quercetin (Q), retinol (R) and coumaric acid (C)) resulted in greater absorbance in the UVB region of the spectrum (blue line Figure 27Figure 27). This can be explained by the fact that all three UV filters absorb in the UVB region and not in the UVA region. In order to achieve a uniform absorbance profile across the entire UV spectrum several attempts were done where different ratios of the UV filters were tested. The total loading was always kept below 10 wt.% because in the work of Hayden *et al.*[22] is found that ECNPs can encapsulate organic UV filters efficiently (~100%) to about 13 wt.%. This meant that the encapsulation efficiency remained ~100% and the absorbance profiles from the ECNPs were reproducible. It was found that a ratio of 7:1.5:1.5 ((Q), (R), (C)) provided uniform coverage of the entire UV spectrum (red line, Figure 27).

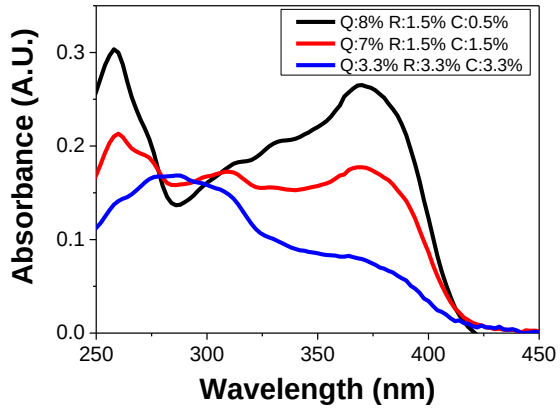

Figure 27: absorption spectra of ECNPs with the three UV filters encapsulated in varying rations in which the total loading was kept under 10 wt.%

4.4.2 Broadband ZNPs

In a second stage was investigated whether the ratio 7:1.5:1.5 (Q, C, R) could also provide broadband UV protection within ZNP. The same anti-solvent precipitation was used as for the individual encapsulation of the UV filters into ZNPs. The prepared dispersion is depicted in Figure 28, together with a dispersion of ZNPs without any UV filter encapsulated.

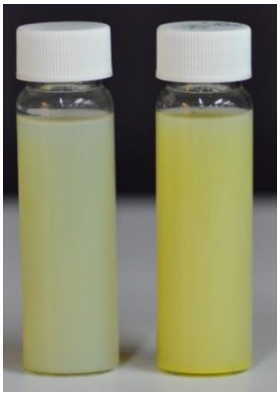

Figure 28: photo of the ZNP dispersion without (left) and with (right) encapsulated UV filters.

Size and stabilisation characterisation

The ZNPs with all three natural UV filters encapsulated had an average particle size of 76 nm and PDI with 0.139 as determined by DLS measurements and confirmed by SEM imaging (Figure 29). A zeta potential of +30 mV (at pH= 3.5) was measured. The dispersion showed colloidal stability at this pH but sedimentation within the dispersion was observed already after a few days at the pH of miliQ water (pH = 5-6). This can be explained by the isoelectric point of zein being at a pH of 6.8.

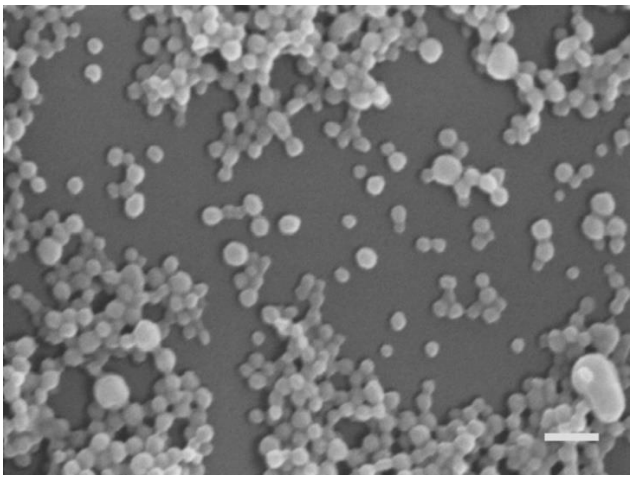

Figure 29: SEM image of ZNPs with all three UV filters encapsulated (scale bar 200 nm)

Absorbance

Figure 30 shows the absorbance spectrum of the broadband UV protective ZNPs with 10 wt.% encapsulated biobased UV filter (ratio 7:1.5:1.5).

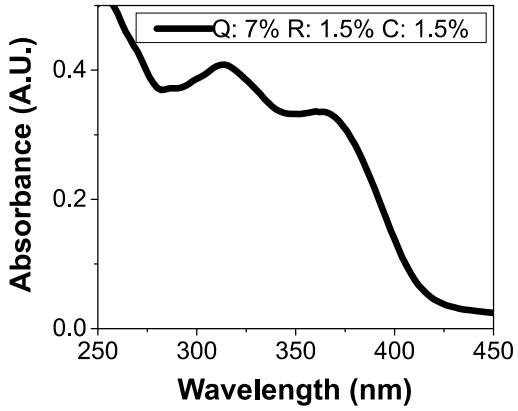

Figure 30: absorption spectrum of ZNPs with encapsulated UV filter, showing a broadband absorbance profile across the UV spectrum.

Interestingly, the absorbance of zein itself slightly contributed to the overall absorbance of the ZNPs which can be seen by comparing the absorbance in Figure 27 (red line) and Figure 30. The absorbance profile remained approximately uniform but slightly greater in the UVB region, as is expected because zein has a broad absorbance across the UV spectrum in which the shorter wavelengths are better absorbed[86]. Only the absorption profile, and not the exact absorbance values, can be compared between Figure 27 (red line) and Figure 30 because although the ratios were equal, the amounts were not – in order to prepare particles of similar

size more zein (thus UV filter too) was used than EC (see experimental section). From Figure 30 can also be seen that the ZNPs absorb at wavelengths greater than 425 nm. This resulted in a distinctive yellow colour of the ZNPs[112] compared to the ECNPs[31] (Figure 25 left vial vs. Figure 28 left vial). The encapsulation of quercetin, which was necessary to achieve absorbance in the UVA region of the spectrum, also gave the dispersions a yellow colour due to its absorbance in the blue region of the visible light spectrum[84]. Therefore, the resultant ECNP and ZNP dispersions both had a yellow colour, but the ZNPs slightly more than the ECNPs (Figure 25 right vial vs. Figure 28 right vial).

4.5 Application of ECNPs: Broadband UV protective coatings

The ability for these UV-absorbing nanoparticles to form coatings is essential for photoprotection applications such as cosmetic sunscreens and packaging materials.

Coatings were prepared from ECNPs by spin coating because of their superior colour and ease of handling with regards to their stability at close-to neutral pH (compared to ZNPs). ECNPs dispersion (30 g L^{-1}) with the UV filters encapsulated in a ratio of 7:1.5:1.5 (Q, R, C) were used because they provide uniform broadband UV coverage. The resulting all-natural coatings were transparent (Figure 31a) and with uniform absorbance profiles across the entire UV spectrum. SEM imaging of the coating confirmed that the particles are homogenously and closely packed on the cover slip (Figure 31b). The absorbance intensity of the coatings can be tuned via the spin coating of subsequent layers on top of the original (Figure 31c).

Despite the prominent yellow colour of the ECNP dispersions, the coating appeared very transparent and a yellow tinge is only visible upon close inspection of the coating at the edges (Figure 31a), due to the well-known 'coffee-ring effect' where higher concentrations of particles end up at the edges in coatings prepared by spin coating[113].

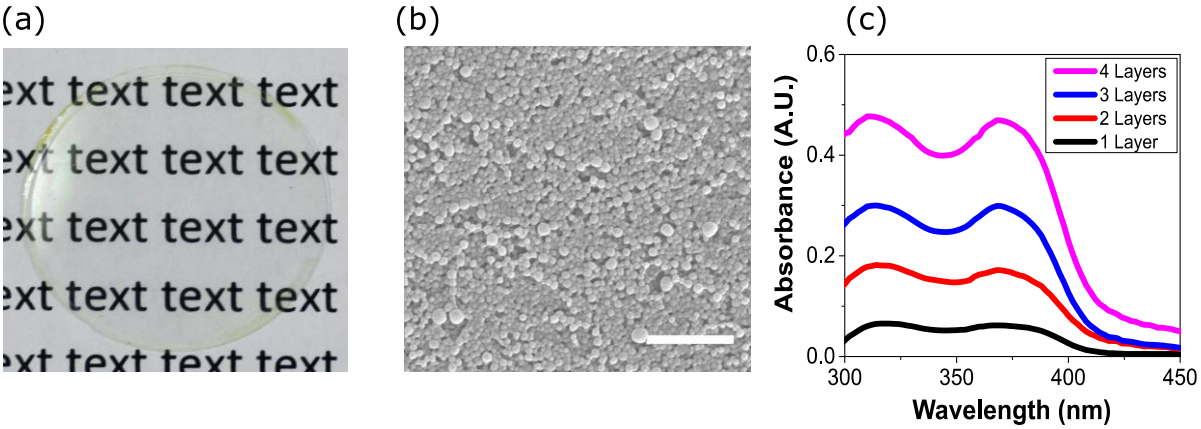

Figure 31: (a) photo of a transparent and uniform coating of the ECNPs on a glass cover slip. (b) SEM images of the coating surface (scale bar 1 micron). (c) absorption spectrum of the ECNP coating showing the absorbance of each successive spin coated layer. Wavelength slower than λ = 300 nm are not shown as they are absorbed by the glass coverslip.

In order to obtain greater absorbance but still maintaining thin coatings, loading of the ECNPs with greater than 10 wt.% material was investigated. Spin coating multiple layers can sometimes result in non-uniform coatings so thinner coatings with already high absorbances are desirable. Higher absorbance could simply be achieved by dissolving more material in the initial ethanol solution, the resulting ECNPs showed a much greater absorbance at the same concentration of particles (Figure 27 vs Figure 32). However, the addition of the UV filters with

total amounts higher than 10 wt.% resulted in uncontrolled and unpredictable encapsulation. Figure 32 depicts the absorbance curves of ECNPs where more than 10 wt.% UV filter was encapsulated. It would have been expected that the addition of the ratio 15:15:4 (Q, R, C) would lead to a higher absorbance than the ratio 10:3:3 (Q, R, C). However, higher absorbance, especially in the absorbance region of retinol, is observed for the latter. This is likely because the ECNPs are unable to encapsulate all material after a certain maximum point, which is consistent with the “Maximum Particle Loading” results in Figure 21, where is found that quercetin can only be encapsulated to a maximum of between 10-14 wt.%.

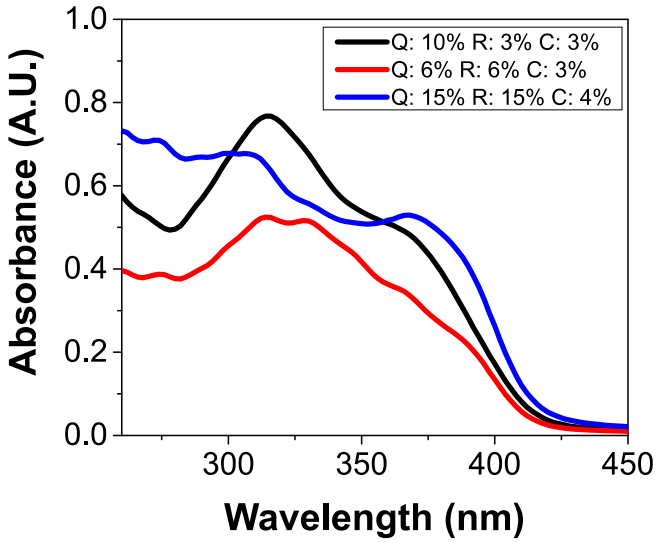

Figure 32: absorption spectra showing coatings of ECNPs with the three UV filters encapsulated in varying ratios,

Thus, in order to obtain greater absorbance but still maintaining thin coatings, spin coatings from the ECNPs with a 15:15:4 (Q, R, C) ratio of encapsulated UV filter were prepared. Figure 33 depicts the absorbance spectra of the subsequent spin coated layers of this dispersion. When comparing Figure 31c with Figure 33 can be seen that spin coating the ECNPs with higher ratios of encapsulated UV filters gives thinner coatings with greater absorbance than an equal concentration (30 g L^{-1}) of the ECNPs with less encapsulated material. The spin coatings were again prepared onto plasma-cleaned, circular glass microscope cover slips at 1800 rpm for 1 minute. This way, highly transparent and thin coatings with a high absorbance could be prepared.

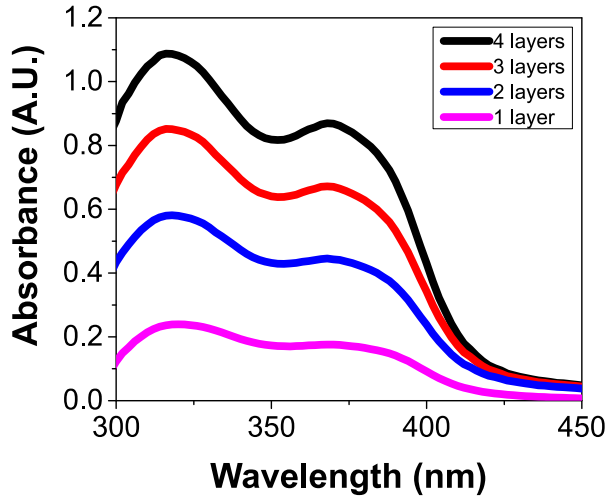

Figure 33: absorption spectrum of ECNP coatings prepared from te ECNPs with a 15:15:4 ratio of encapsulated quercetin, retinol and coumaric acid. The absorbance is shown for 4 successive spin coated layers. Wavelengths lower than λ = 300 nm are not shown as they are absorbed by the glass coverslip.

Photo stability of coatings

Sunscreens products containing UV-filters are used worldwide to protect from the harmful effects of UV light. However, in order to provide this photoprotective function, it is desirable if they are also photostable. Effective photo stability is therefore essential for these coatings if they are to become commercially viable. Furthermore, the photo stability is known to vary greatly between commercialised UV filters[70,114,115] and even though sunscreens are regulated in most countries, photo stability testing is not always mandatory[116]. In order to investigate the photo stability of the all-natural UV-absorbing ECNPs, the coating from Figure 31c with a ratio of 7:1.5:1.5 (Q, C, R) was irradiated by artificial sunlight for 4 hours and the coating absorbance was measured at hourly intervals (Figure 34).

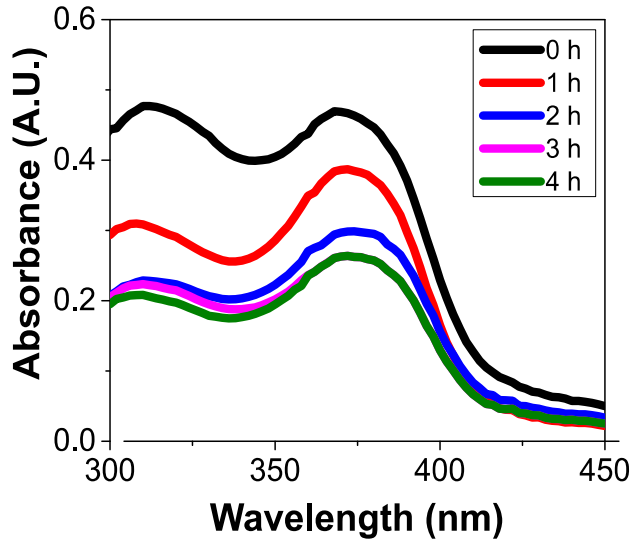

Figure 34: absorption spectrum showing the degradation of the absorbance of the ECNPs when irritated by artificial sunlight for 4h.

The coating was subjected to a total flux of 432 kJ m^{-2} UV irradiation (λ=300-400 nm) over the 4 hours which translates to 2 hours and 24 minutes of summer sunlight in Nice (France) at noon[99]. The coating absorbance degraded approximately 50% after the total 4 hours of irradiation. This degradation is about two times as large as what is reported for ECNPs with encapsulated synthetic organic UV filters[22]. Interestingly, the coating begins to degrade very quickly but this degradation then plateaus after about 2 hours of irradiation. This is likely due to the fast degradation of retinol, which is known to be quite unstable compared to quercetin and coumaric acid[114]. This hypothesis is supported by the fact that the coating degrades more in the UVB region (as opposed to UVA) of the UV spectrum – where retinol absorbs. The coating does maintain uniform absorbance across the entire UV spectrum and, therefore, it can be concluded that these all-natural UV-absorbing ECNPs can be used to prepare effective UV protective coatings with photodegradation values comparable with non-biobased UV filters.

5 Conclusion and outlook

In this work we prepared UV absorbing nanoparticles with an all-natural composition via the encapsulation of biobased photoprotectants into nanoparticles from ethyl cellulose and zein. In a first stage the individual encapsulation of three biobased photoprotectants (coumaric acid, retinol and quercetin) into nanoparticles from ethyl cellulose was studied. We found that all three filters could be physically and efficiently encapsulated (up to a maximum of 13 wt.%) with retinol being the most efficient, and increasing loadings of quercetin and retinol resulted in more favourable behaviour (than large amounts of coumaric acid) where the particle size remained unchanged and the absolute zeta potential (thus dispersion stability) increased from -25 mV to -35 mV. Upon loading of *p*-coumaric acid, the size of the ECNPs increased from 70 to 140 nm, and the zeta potential increased from -25 mV to -8 mV. The biobased photoprotectants were effectively retained inside the ECNPs at rates comparable to synthetic UV filters encapsulated for sunscreen applications.

In a second stage, broadband UV absorbing nanoparticles of ethyl cellulose and zein with all three filters encapsulated were prepared. The composition of the ECNPs and ZNPs could be easily tuned in order to exhibit uniform, broadband UV spectrum absorbance profiles. The functionalized ECNPs dispersions were then spin coated to prepare all-natural, transparent coatings with broadband and tuneable absorbance. The coatings appeared to have similar photo stability values as non-biobased UV filters.

Photoprotection technology is pushing towards biobased alternatives for inorganic and synthetic organic UV filters because of their association with many adverse health and environmental effects. Here, effective all-natural UV-absorbing nanoparticles are developed, representing significant progress towards potentially satisfying these issues.

It has already be shown that quercetin and rutin (quercetin's glucoside) give similar SPF (Sun Protection Factor) values as, the synthetic sunscreen agent homosalate when incorporated in oil-in-water emulsions and when used in association with titanium dioxide a SPF of 30 was obtained[117]. For these biobased UV filters to be commercially available, high enough SPFs values (>30) should be obtained. When SPFs are not high enough the addition of small amounts of titanium dioxide within the particle could be studied.

In this study is chosen to work with the three biobased photoprotectants coumaric acid, retinol and quercetin because together they cover the entire UV spectrum. However, there are more polyphenols or carotenoids which can be studied. This also counts for the carrier materials (in

this work EC and zein are used). It has been observed that the encapsulation by ECNPs of large amounts of coumaric acid is slightly different from the other two UV filters which might be attributed due to the charge on coumaric acid. In particular interesting could thus be the encapsulation mechanism between a charged biopolymer and charged photoprotectant. Nanoparticles are also used as stabilizers in Pickering emulsions. ECNPs have very recently been explored as stabilizers for oil in water Pickering emulsions by Wu *et al*.[118], where alterations (by acids/base and salt) in the surface charge of the ECNPs determined the stability. Functionalized ECNPs as stabilizers for Pickering emulsions could also be explored, where it is especially interesting to see what happens with the stability when the functionalized particles carry a charge.

Acknowledgements

I would like to extend my gratitude to many people who assisted in the completion of this work. First and foremost, I would like to thank my daily supervisor Douglas Hayden for guidance along the way and constant willingness and availability to discuss any aspect of the work. I really enjoyed co-working with you, your pleasant and relaxed personality made it very easy and enjoyable to work on this project. I would also like to thank you for your critical remarks and eye for detail improving this thesis and my presentations. Writing the article, based on this work, together with you and your comments on this thesis and my final presentation also improved my writing and presentation skills in general.

I also thank Arnout Imhof and Krassimir Velikov for their input and ideas during Friday afternoon meetings. Krassimir I would like to thank you as well for your effort to help me finding an internship at Unilever, I'm really looking forward to the internship in Shanghai.

Finally, I would like to thank everyone in the Soft Condensed Matter group for making me feel welcome and always friendly advice. A special thanks to everyone in the student room for the great time.

Bibliography

1. Lipson, M. Overcoming the limitations of microelectronics using Si nanophotonics: solving the coupling, modulation and switching challenges. *Nanotechnology* **15,** S622–S627 (2004).

2. Gandomi, N. *et al.* Solid lipid nanoparticles surface modified with anti-Contactin-2 or anti-Neurofascin for brain-targeted delivery of medicines. *Pharm. Dev. Technol.* **22,** 426–435 (2017).

3. Farokhzad, O. C. & Langer, R. Impact of Nanotechnology on Drug Delivery. *ACS Nano* **3,** 16–20 (2009).

4. Shi, J., Votruba, A. R., Farokhzad, O. C. & Langer, R. Nanotechnology in Drug Delivery and Tissue Engineering: From Discovery to Applications. *Nano Lett.* **10,** 3223–3230 (2010).

5. Weiss, J., Takhistov, P. & McClements, D. J. Functional materials in food nanotechnology. *J. Food Sci.* **71,** 107–116 (2006).

6. Joye, I. J. & McClements, D. J. Biopolymer-based nanoparticles and microparticles: Fabrication, characterization, and application. *Current Opinion in Colloid and Interface Science* **19,** 417–427 (2014).

7. Joye, I. J. & McClements, D. J. Production of nanoparticles by anti-solvent precipitation for use in food systems. *Trends in Food Science and Technology* **34,** 109–123 (2013).

8. Davidov-Pardo, G., Joye, I. J. & Mcclements, D. J. Encapsulation of resveratrol in biopolymer particles produced using liquid antisolvent precipitation. Part 1: Preparation and characterization. *Food Hydrocoll.* **45,** 309–316 (2015).

9. Shi, L., Shan, J., Ju, Y., Aikens, P. & Prud 'homme, R. K. Nanoparticles as delivery vehicles for sunscreen agents. *Colloids Surfaces A Physicochem. Eng. Asp.* **396,** 122–129 (2011).

10. Raj, S., Jose, S., Sumod, U. S. & Sabitha, M. Nanotechnology in cosmetics: Opportunities and challenges. *J. Pharm. Bioallied Sci.* **4,** 186–93 (2012).

11. Babu, R. P., O'Connor, K. & Seeram, R. Current progress on bio-based polymers and their future trends. *Prog. Biomater.* **2,** 8 (2013).

12. Elsabee, M. Z. & Abdou, E. S. Chitosan based edible films and coatings: A review. *Materials Science and Engineering C* **33,** 1819–1841 (2013).

13. Cutter, C. N. Opportunities for bio-based packaging technologies to improve the quality and safety of fresh and further processed muscle foods. *Meat Sci.* **74,** 131–142 (2006).

14. Cooksey, K. *Antimicrobial food packaging materials*. *Additives for Polymers* **2001,** (2001).

15. Andrew N. Shipway Eugenii Katz, I. W. Nanoparticle Arrays on Surfaces for Electronic, Optical, and Sensor Applications. *ChemPhysChem* **1,** 18–52 (2000).

16. Bell, N. S. & Piech, M. Photophysical Effects between Spirobenzopyran−Methyl methacrylate-Functionalized Colloidal Particles. *Langmuir* **22,** 1420–1427 (2006).

17. Ren, Y., Chen, M., Zhang, Y. & Wu, L. Fabrication of rattle-type TiO2/SiO2core/shell particles with

both high photoactivity and UV-shielding property. *Langmuir* **26,** 11391–11396 (2010).

18. Patel, A. R., Heussen, P. C. M., Hazekamp, J., Drost, E. & Velikov, K. P. Quercetin loaded biopolymeric colloidal particles prepared by simultaneous precipitation of quercetin with hydrophobic protein in aqueous medium. *Food Chem.* **133,** 423–9 (2012).

19. Deng, Y. *et al.* A sunblock based on bioadhesive nanoparticles. *Nat. Mater.* **14,** 1278–1285 (2015).

20. Wang, S., Balagula, Y. & Osterwalder, U. Photoprotection: a review of the current and future technologies. *Dermatol. Ther.* **23,** 31–47 (2010).

21. Tolbert, S. H., McFadden, P. D. & Loy, D. A. New Hybrid Organic/Inorganic Polysilsesquioxane–Silica Particles as Sunscreens. *ACS Appl. Mater. Interfaces* **8,** 3160–3174 (2016).

22. Hayden, D. R., Imhof, A. & Velikov, K. P. Biobased Nanoparticles for Broadband UV Protection with Photostabilized UV Filters. *ACS Appl. Mater. Interfaces* **8,** 32655–32660 (2016).

23. Downs, C. A. *et al.* Toxicopathological Effects of the Sunscreen UV Filter, Oxybenzone (Benzophenone-3), on Coral Planulae and Cultured Primary Cells and Its Environmental Contamination in Hawaii and the U.S. Virgin Islands. *Arch. Environ. Contam. Toxicol.* **70,** 265–288 (2016).

24. Cerqueira, M. A. *et al.* Design of Bio-nanosystems for Oral Delivery of Functional Compounds. doi:10.1007/s12393-013-9074-3

25. Buzea, C., Pacheco, I. I. & Robbie, K. Nanomaterials and nanoparticles: Sources and toxicity. *Biointerphases* **2,** MR17-MR71 (2007).

26. Christian, P., Von der Kammer, F., Baalousha, M. & Hofmann, T. Nanoparticles: structure, properties, preparation and behaviour in environmental media. *Ecotoxicology* **17,** 326–343 (2008).

27. Sugimoto, T. Preparation of monodispersed colloidal particles. *Adv. Colloid Interface Sci.* **28,** 65–108 (1987).

28. Plasari, E., Grisoni, P. & Villermaux, J. Influence of Process Parameters on the Precipitation of Organic Nanoparticles by Drowning-Out. *Chem. Eng. Res. Des.* **75,** 237–244 (1997).

29. Horn, D. & Rieger, J. Organic Nanoparticles in the Aqueous Phase—Theory, Experiment, and Use. *Angew. Chemie Int. Ed.* **40,** 4330 (2001).

30. Aubry, J., Ganachaud, F., Cohen Addad, J.-P. & Cabane, B. Nanoprecipitation of Polymethylmethacrylate by Solvent Shifting:1. Boundaries. *Langmuir* **25,** 1970–1979 (2009).

31. Bizmark, N., Ioannidis, M. A. & Henneke, D. E. Irreversible Adsorption-Driven Assembly of Nanoparticles at Fluid Interfaces Revealed by a Dynamic Surface Tension Probe. *Langmuir* **30,** 710–717 (2014).

32. Jin, H. *et al.* Super stable foams stabilized by colloidal ethyl cellulose particles. doi:10.1039/c1sm06518a

33. Pan-In, P., Banlunara, W., Chaichanawongsaroj, N. & Wanichwecharungruang, S. Ethyl cellulose nanoparticles: Clarithomycin encapsulation and eradication of H. pylori. *Carbohydr. Polym.* **109,** 22–27 (2014).

34. Lokhande, A. B., Mishra, S., Kulkarni, R. D. & Naik, J. B. Preparation and characterization of repaglinide loaded ethylcellulose nanoparticles by solvent diffusion

technique using high pressure homogenizer. *J. Pharm. Res.* **7,** 421–426 (2013).

35. Langer, K. *et al.* Optimization of the preparation process for human serum albumin (HSA) nanoparticles. *Int. J. Pharm.* **257,** 169–180 (2003).

36. Wang, H. *et al.* Amphiphilic dextran derivatives nanoparticles for the delivery of mitoxantrone. *J. Appl. Polym. Sci.* **126,** E35–E43 (2012).

37. Taheri, E. S., Jahanshahi, M. & Mosavian, M. T. H. Preparation, Characterization and Optimization of Egg Albumin Nanoparticles as Low Molecular-Weight Drug Delivery Vehicle. *Part. Part. Syst. Charact.* **29,** 211–222 (2012).

38. Khan, S. A. & Schneider, M. Improvement of Nanoprecipitation Technique for Preparation of Gelatin Nanoparticles and Potential Macromolecular Drug Loading. *Macromol. Biosci.* **13,** 455–463 (2013).

39. Thorat, A. A. & Dalvi, S. V. Liquid antisolvent precipitation and stabilization of nanoparticles of poorly water soluble drugs in aqueous suspensions: Recent developments and future perspective. *Chem. Eng. J.* **181–182,** 1–34 (2011).

40. Reverchon, E. Supercritical antisolvent precipitation of micro-and nano-particles. *J. Supercrit. Fluids* **15,** 1–21 (1999).

41. Montes, A., Gordillo, M. D., Pereyra, C. & Martínez De La Ossa, E. J. Co-precipitation of amoxicillin and ethyl cellulose microparticles by supercritical antisolvent process. in *Journal of Supercritical Fluids* **60,** 75–80 (Elsevier, 2011).

42. Rogers, T. L. *et al.* Development and characterization of a scalable controlled precipitation process to enhance the dissolution of poorly water-soluble drugs. *Pharm. Res.* **21,** 2048–2057 (2004).

43. Matteucci, M. E., Hotze, M. A., Johnston, K. P. & Williams, R. O. Drug nanoparticles by antisolvent precipitation: Mixing energy versus surfactant stabilization. *Langmuir* **22,** 8951–8959 (2006).

44. Sugimoto, T. Formation of Monodispersed Nano- and Micro-Particles Controlled in Size, Shape, and Internal Structure. *Chem. Eng. Technol.* **26,** 313–321 (2003).

45. Weber, M., Russell, L. M. & Debenedetti, P. G. Mathematical modeling of nucleation and growth of particles formed by the rapid expansion of a supercritical solution under subsonic conditions. *J. Supercrit. Fluids* **23,** 65–80 (2002).

46. Weber, M. & Thies, M. C. *Supercritical Fluid Technology in Materials Science and Engineering*. (Marcel dekker, 2002).

47. Mccabe, W. ., Smith, J. . & Harriot, P. *Unit operations of Chemical Engineering*. (McGraw-Hill, 2001).

48. Chan, H.-K., Chi, P. & Kwok, L. Production methods for nanodrug particles using the bottom-up approach ☆. *Adv. Drug Deliv. Rev.* **63,** 406–416 (2011).

49. Park, M. W. & Yeo, S. Do. Antisolvent crystallization of roxithromycin and the effect of ultrasound. *Sep. Sci. Technol.* **45,** 1402–1410 (2010).

50. Lonare, A. A. & Patel, S. R. Antisolvent Crystallization of Poorly Water Soluble Drugs. *Int. J. Chem. Eng. Appl.* **4,** 337–341 (2013).

51. Kakran, M., Sahoo, N. G., Tan, I. L. & Li, L. Preparation of nanoparticles of poorly water-soluble antioxidant curcumin by antisolvent precipitation methods. *J. Nanoparticle Res.* **14,** (2012).

52. Park, S. J., Jeon, S. Y. & Yeo, S. Do.

Recrystallization of a pharmaceutical compound using liquid and supercritical antisolvents. *Ind. Eng. Chem. Res.* **45,** 2287–2293 (2006).

53. Baldyga, J., Podgorska, W. & Pohorecki, R. Mixing-precipitation model with application to double feed semibatch precipitation. *Chem. Enqineerino Sci.* **50,** 1281–1300 (1995).

54. Zhao, H., Wang, J. X., Wang, Q. A., Chen, J. F. & Yun, J. Controlled liquid antisolvent precipitation of hydrophobic pharmaceutical nanoparticles in a MicroChannel reactor. *Ind. Eng. Chem. Res.* **46,** 8229–8235 (2007).

55. Zhang, Z.-B. *et al.* Nanonization of Megestrol Acetate by Liquid Precipitation. *Ind. Eng. Chem. Res.* **48,** 8493–8499 (2009).

56. Wang, J., Zhao, M., Yang, X. & Jiang, Y. Improvement on functional properties of wheat gluten by enzymatic hydrolysis and ultrafiltration. *J. Cereal Sci.* **44,** 93–100 (2006).

57. Serpone, N., Dondi, D. & Albini, A. Inorganic and organic UV filters: Their role and efficacy in sunscreens and suncare products. *Inorganica Chim. Acta* **360,** 794–802 (2007).

58. Rossi, L., Seijen ten Hoorn, J. W. M., Melnikov, S. M. & Velikov, K. P. Colloidal phytosterols: synthesis, characterization and bioaccessibility. *Soft Matter* **6,** 928–936 (2010).

59. Zhang, J. Y. *et al.* Preparation of amorphous cefuroxime axetil nanoparticles by controlled nanoprecipitation method without surfactants. *Int. J. Pharm.* **323,** 153–160 (2006).

60. Patel, A., Hu, Y., Tiwari, J. K. & Velikov, K. P. Synthesis and characterisation of zein–curcumin colloidal particles. *Soft Matter* **6,** 6192 (2010).

61. Mahnaj, T., Ahmed, S. U. & Plakogiannis, F. M. Characterization of ethyl cellulose polymer. *Pharm. Dev. Technol.* **18,** 982–989 (2013).

62. Bizmark, N. & Ioannidis, M. A. Effects of Ionic Strength on the Colloidal Stability and Interfacial Assembly of Hydrophobic Ethyl Cellulose Nanoparticles. *Langmuir* **31,** 9282–9289 (2015).

63. Zhong, Q. & Jin, M. Zein nanoparticles produced by liquid–liquid dispersion. *Food Hydrocoll.* **23,** 2380–2387

64. Mora-Huertas, C. E., Fessi, H. & Elaissari, A. Influence of process and formulation parameters on the formation of submicron particles by solvent displacement and emulsification-diffusion methods: Critical comparison. *Adv. Colloid Interface Sci.* **163,** 90–122 (2011).

65. Beck, C., Dalvi, S. V, Dave, R. N. & York, O. H. Controlled liquid antisolvent precipitation using a rapid mixing device. *Chem. Eng. Sci.* **65,** 5669–5675 (2010).

66. Kakran, M. *et al.* Fabrication of drug nanoparticles by evaporative precipitation of nanosuspension. *Int. J. Pharm.* **383,** 285–292 (2010).

67. Meer, T. A., Sawant, K. P. & Amin, P. D. Liquid antisolvent precipitation process for solubility modulation of bicalutamide. *Acta Pharm.* **61,** 435–445 (2011).

68. Aschenbrenner, E. *et al.* Using the polymeric ouzo effect for the preparation of polysaccharide-based nanoparticles. *Langmuir* **29,** 8845–8855 (2013).

69. Stavros, V. G. Photochemistry: A bright future for sunscreens. *Nat. Chem.* **6,** 955–956 (2014).

70. Bens, G. in *Sunlight, Vitamin D and Skin Cancer* 429–463 (2014).

71. Norval, M. *et al.* The human health

effects of ozone depletion and interactions with climate change. *Photochem. Photobiol. Sci.* **10,** 199 (2011).

72. Danovaro, R. *et al.* Sunscreens cause coral bleaching by promoting viral infections. *Environ. Health Perspect.* **116,** 441–447 (2008).

73. Sanchez-Quiles, D. & Tovar-Sanchez, A. Sunscreens as a Source of Hydrogen Peroxide Production in Coastal Waters. *Environ. Sci. Technol.* **48,** 9037–9042 (2014).

74. Hund-Rinke, K. & Simon, M. Ecotoxic Effect of Photocatalytic Active Nanoparticles (TiO2) on Algae and Daphnids. *Environ. Sci. Pollut. Res.* **13,** 225–232 (2006).

75. Kümmerer, K., Menz, J., Schubert, T. & Thielemans, W. Biodegradability of organic nanoparticles in the aqueous environment. *Chemosphere* **82,** 1387–1392 (2011).

76. Hanson, K. M., Gratton, E. & Bardeen, C. J. Sunscreen enhancement of UV-induced reactive oxygen species in the skin. *Free Radic. Biol. Med.* **41,** 1205–1212 (2006).

77. Maier, T. & Korting, H. C. Sunscreens - Which and what for? *Skin Pharmacol. Physiol.* **18,** 253–262 (2005).

78. Krause, M. *et al.* Sunscreens: are they beneficial for health? An overview of endocrine disrupting properties of UV-filters. *Int. J. Androl.* **35,** 424–436 (2012).

79. Oliveira, C. A. De *et al.* Cutaneous biocompatible rutin-loaded gelatin-based nanoparticles increase the SPF of the association of UVA and UVB filters. *Eur. J. Pharm. Sci.* **81,** 1–9 (2016).

80. Latif, R., Refai, H. & Tawakkol, S. Photostabilization of sunscreen oil through preparation of a free-flowing powder. *J. Microencapsul.* **28,** 159–165 (2011).

81. Perugini, P. *et al.* Effect of nanoparticle encapsulation on the photostability of the sunscreen agent, 2-ethylhexyl-p-methoxycinnamate. *Int. J. Pharm.* **246,** 37–45 (2002).

82. Wissing, S. A. & Muller, R. H. Solid lipid nanoparticles as carrier for sunscreens: in vitro release and in vivo skin penetration. *J. Control. Release* **81,** 225–233 (2002).

83. Herzog, B., Hüglin, D., Borsos, E., Stehlin, A. & Luther, H. New UV absorbers for cosmetic sunscreens - A breakthrough for the photoprotection of human skin. *Chimia (Aarau).* **58,** 554–559 (2004).

84. Cefali, L. C., Ataide, J. A., Moriel, P., Foglio, M. A. & Mazzola, P. G. Plant-based active photoprotectants for sunscreens. *International Journal of Cosmetic Science* **38,** 346–353 (2016).

85. Tan, Q., Liu, W., Guo, C. & Zhai, G. Preparation and evaluation of quercetin-loaded lecithin-chitosan nanoparticles for topical delivery. *Int. J. Nanomedicine* **6,** 1621–1630 (2011).

86. Sessa, D. J., Eller, F. J., Palmquist, D. E. & Lawton, J. W. Improved methods for decolorizing corn zein. *Ind. Crops Prod.* **18,** 55–65 (2003).

87. Liu, Z., Huang, Y., Jin, Y. & Cheng, Y. Mixing intensification by chaotic advection inside droplets for controlled nanoparticle preparation. *Microfluid. Nanofluidics* **9,** 773–786 (2010).

88. Patel, A., Hu, Y., Tiwari, J. K. & Velikov, K. P. Synthesis and characterisation of zein–curcumin colloidal particles. *Soft Matter* **6,** 6192 (2010).

89. Nichols, J. A. & Katiyar, S. K. Skin

photoprotection by natural polyphenols: Anti-inflammatory, antioxidant and DNA repair mechanisms. *Archives of Dermatological Research* **302,** 71–83 (2010).

90. Fang, Z. & Bhandari, B. Encapsulation of polyphenols - a review. *Trends in Food Science and Technology* **21,** 510–523 (2010).

91. Smith, M. M. & Hartley, R. D. Occurrence and nature of ferulic acid substitution of cell-wall polysaccharides in graminaceous plants. *Carbohydr. Res.* **118,** 65–80 (1983).

92. Beecher, G. R. Overview of dietary flavonoids: nomenclature, occurrence and intake. *J. Nutr.* **133,** 3248S–3254S (2003).

93. Agati, G. & Tattini, M. Multiple functional roles of flavonoids in photoprotection. *New Phytol.* **186,** 786–793 (2010).

94. Sisa, M., Bonnet, S. L., Ferreira, D. & Van der Westhuizen, J. H. Photochemistry of Flavonoids. *Molecules* **15,** 5196–5245 (2010).

95. Rutz, J. K. *et al.* Microencapsulation of purple Brazilian cherry juice in xanthan, tara gums and xanthan-tara hydrogel matrixes. *Carbohydr. Polym.* **98,** 1256–1265 (2013).

96. Varani, J. *et al.* Vitamin A Antagonizes Decreased Cell Growth and Elevated Collagen-Degrading Matrix Metalloproteinases and Stimulates Collagen Accumulation in Naturally Aged Human Skin 1. *J Invest Dermatol* **114,** 480–486 (2000).

97. Antille, C. *et al.* Vitamin A Exerts a Photoprotective Action in Skin by Absorbing Ultraviolet B Radiation. *J. Invest. Dermatol.* **121,** 1163–1167 (2003).

98. de Folter, J. W. J., van Ruijven, M. W. M. & Velikov, K. P. Oil-in-water Pickering emulsions stabilized by colloidal particles from the water-insoluble protein zein. *Soft Matter* **8,** 6807 (2012).

99. Séite, S. *et al.* Mexoryl® SX: A broad absorption UVA filter protects human skin from the effects of repeated suberythemal doses of UVA. *J. Photochem. Photobiol. B Biol.* **44,** 69–76 (1998).

100. Thünemann, A. F. & Beyermann, J. Polyethylenimine complexes with retinoic acid: Structure, release profiles, and nanoparticles. *Macromolecules* **33,** 6878–6885 (2000).

101. Kim, D. G. *et al.* Retinol-encapsulated low molecular water-soluble chitosan nanoparticles. *Int. J. Pharm.* **319,** 130–138 (2006).

102. Patravale, V. B., Date, A. A. & Kulkarni, R. M. Nanosuspensions: a promising drug delivery strategy. *J. Pharm. Pharmacol.* **56,** 827–840 (2004).

103. Kort, R. *et al.* Evidence for trans-cis isomerization of the p-coumaric acid chromophore as the photochemical basis of the photocycle of photoactive yellow protein. *FEBS Lett.* **382,** 73–78 (1996).

104. Suthar, V., Pratap, A. & Raval, H. Studies on poly (hydroxy alkanoates)/(ethylcellulose) blends. *Bull. Mater. Sci* **23,** 215–219 (2000).

105. Williams, D. & Fleming, I. *Spectroscopic methods in organic chemistry*. (Tata McGraw-hill, 2011).

106. Biswick, T., Park, D. H., Shul, Y. G. & Choy, J. H. P-coumaric acid-zinc basic salt nanohybrid for controlled release and sustained antioxidant activity. *J. Phys. Chem. Solids* **71,** 647–649 (2010).

107. Tolbert, S. H., McFadden, P. D. & Loy, D. A. New Hybrid Organic/Inorganic Polysilsesquioxane-Silica Particles

as Sunscreens. *ACS Appl. Mater. Interfaces* **8,** (2016).

108. Kumari, A., Yadav, S. K., Pakade, Y. B., Singh, B. & Yadav, S. C. Development of biodegradable nanoparticles for delivery of quercetin. *Colloids Surfaces B Biointerfaces* **80,** 184–192 (2010).

109. Lautenschlager, S., Wulf, H. . & Pittelkow, M. R. Photoprotection. *Lancet* **370,** 528 (2007).

110. Kidsaneepoiboon, P., Wanichwecharungruang, S. P., Chooppawa, T., Deephum, R. & Panyathanmaporn, T. Organic–inorganic hybrid polysilsesquioxane nanospheres as UVA/UVB absorber and fragrance carrier. *J. Mater. Chem.* **21,** 7922 (2011).

111. Lacatusu, I. *et al.* Design of soft lipid nanocarriers based on bioactive vegetable oils with multiple health benefits. *Chem. Eng. J.* **246,** 311–321 (2014).

112. Patel, A. R. & Velikov, K. P. Zein as a source of functional colloidal nano- and microstructures. *Current Opinion in Colloid and Interface Science* **19,** 450–458 (2014).

113. Yunker, P. J., Still, T., Lohr, M. A. & Yodh, A. G. Suppression of the coffee-ring effect by shape-dependent capillary interactions. *Nature* **476,** 308–311 (2011).

114. Tolleson, W. H. *et al.* Photodecomposition and phototoxicity of natural retinoids. *Int. J. Environ. Res. Public Health* **2,** 147–155 (2005).

115. Morabito, K., Shapley, N. C., Steeley, K. G. & Tripathi, A. Review of sunscreen and the emergence of non-conventional absorbers and their applications in ultraviolet protection. *Int. J. Cosmet. Sci.* **33,** 385–390 (2011).

116. Kockler, J., Oelgemöller, M., Robertson, S. & Glass, B. D. Photostability of sunscreens. *J. Photochem. Photobiol. C Photochem. Rev.* **13,** 91–110 (2012).

117. Choquenet, B., Couteau, C., Paparis, E. & Coiffard, L. J. M. Quercetin and rutin as potential sunscreen agents: Determination of efficacy by an in vitro method. *J. Nat. Prod.* **71,** 1117–1118 (2008).

118. Wu, X. *et al.* Ethyl cellulose nanodispersions as stabilizers for oil in water Pickering emulsions. *Sci. Rep.* **7,** 12079 (2017).

Appendix A

Table A1: Raw data set for Figure 4

Conc. of EC in ethanol (g mL^{-1})	Particle size modal average (nm)	Particle size mean average (nm)	Particle size error (modal average, nm)	Particle size error (mean average, nm)	PDI	PDI diameter (nm)	Yield average (%)	Yield error (%)
1.60 ×10^{-3}	**35**	**50**	**0.197**	**0.280**	**0.230**	**23.7**	**-**	**-**
2.00 ×10^{-3}	**37**	**58**	**0.639**	**0.540**	**0.280**	**30.9**	**-**	**-**
2.75 ×10^{-3}	**39**	**53**	**0.630**	**0.784**	**0.204**	**23.9**	**94.5**	**5.5**
5.50 ×10^{-3}	**64**	**71**	**0.277**	**0.389**	**0.158**	**27.4**	**82.0**	**4.0**
1.00 ×10^{-2}	**87**	**100**	**0.239**	**0.373**	**0.157**	**39.3**	**77.0**	**0.5**
1.50 ×10^{-2}	**113**	**118**	**0.921**	**1.164**	**0.135**	**42.4**	**53.6**	**9.6**
2.00 ×10^{-2}	**148**	**146**	**0.176**	**0.224**	**0.126**	**52.8**	**35.5**	**0.5**
2.25 ×10^{-2}	**177**	**160**	**0.265**	**0.482**	**0.136**	**60.7**	**23.0**	**1.0**
2.50 ×10^{-2}	**206**	**165**	**5.231**	**1.064**	**0.243**	**83.1**	**14.7**	**7.8**

Appendix B

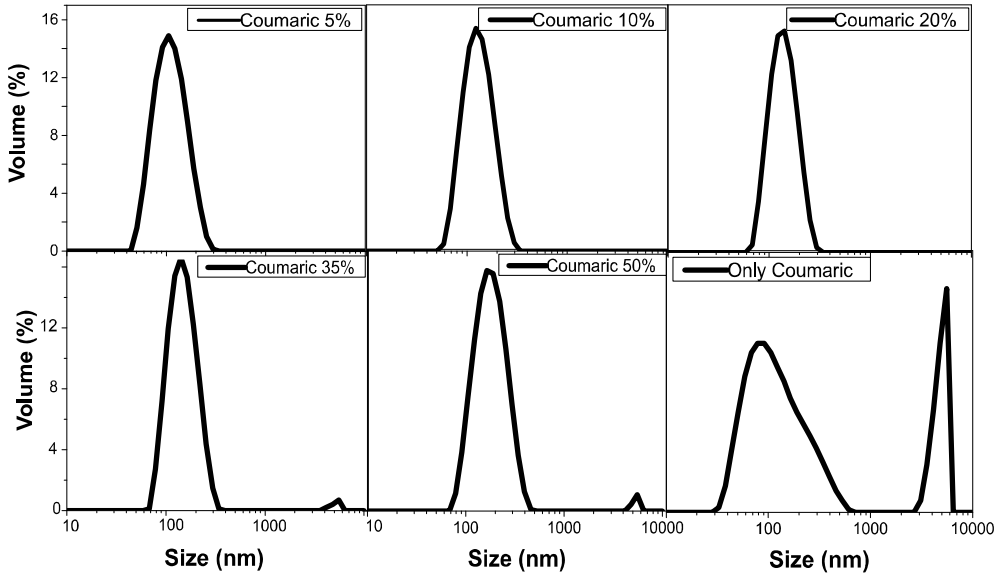

figure B1: volume weighted size distributions as measured by DLS for the ECNP dispersions with encapsulated quercetin in Figure 17.

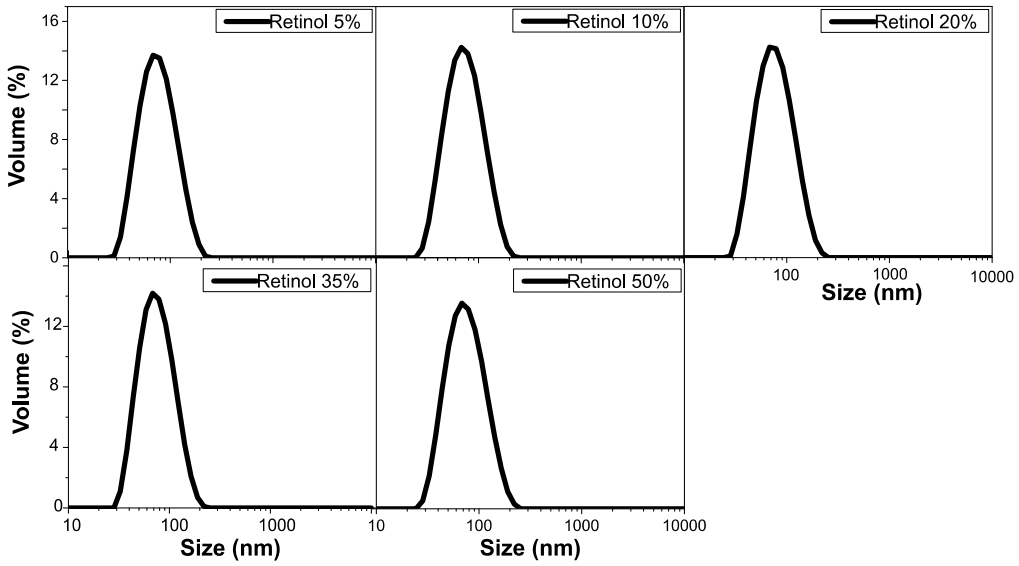

figure B2: volume weighted size distributions as measured by DLS for the ECNP dispersions with encapsulated retinol in Figure 17.

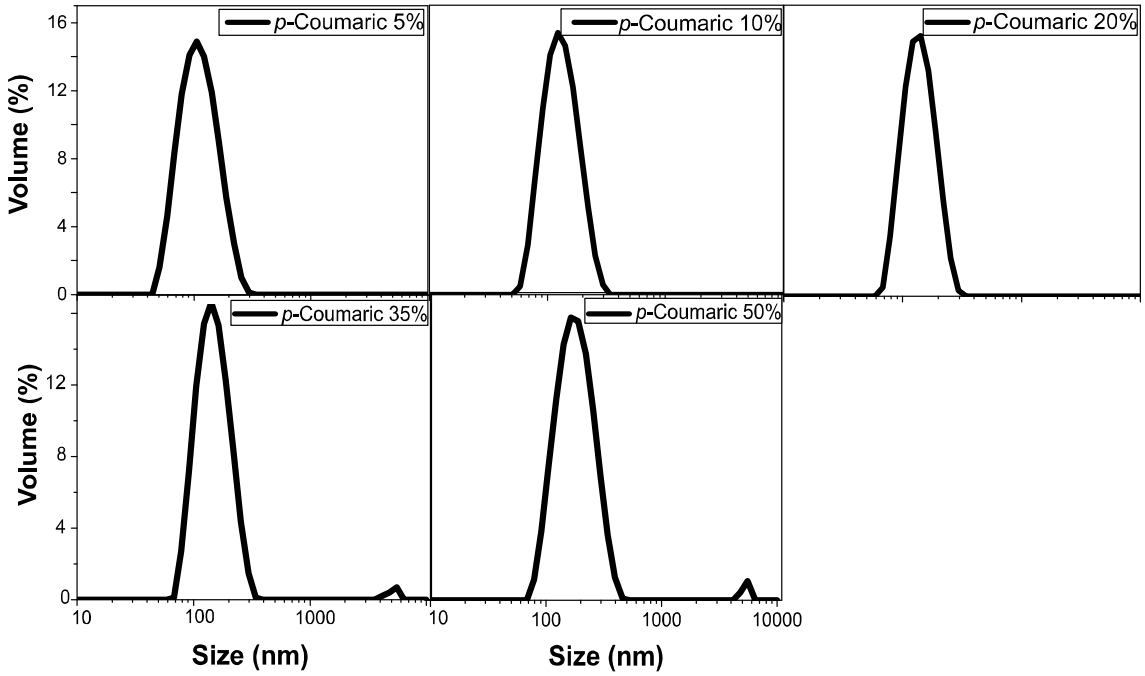

figure B3: volume weighted size distributions as measured by DLS for the ECNP dispersions with encapsulated coumaric acid in Figure 17.

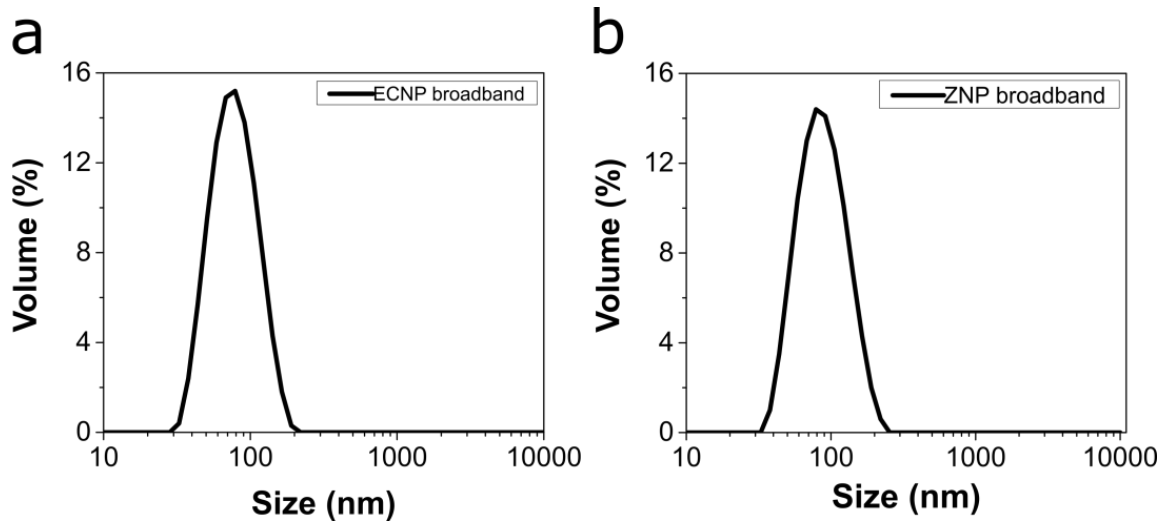

figure B4: volume weighted size distributions as determined by DLS for the (a) ECNPs and (b) ZNPs with quercetin, retinol and coumaric acid encapsulated in the ratio 7:1.5:1.5.

Appendix C

(a)

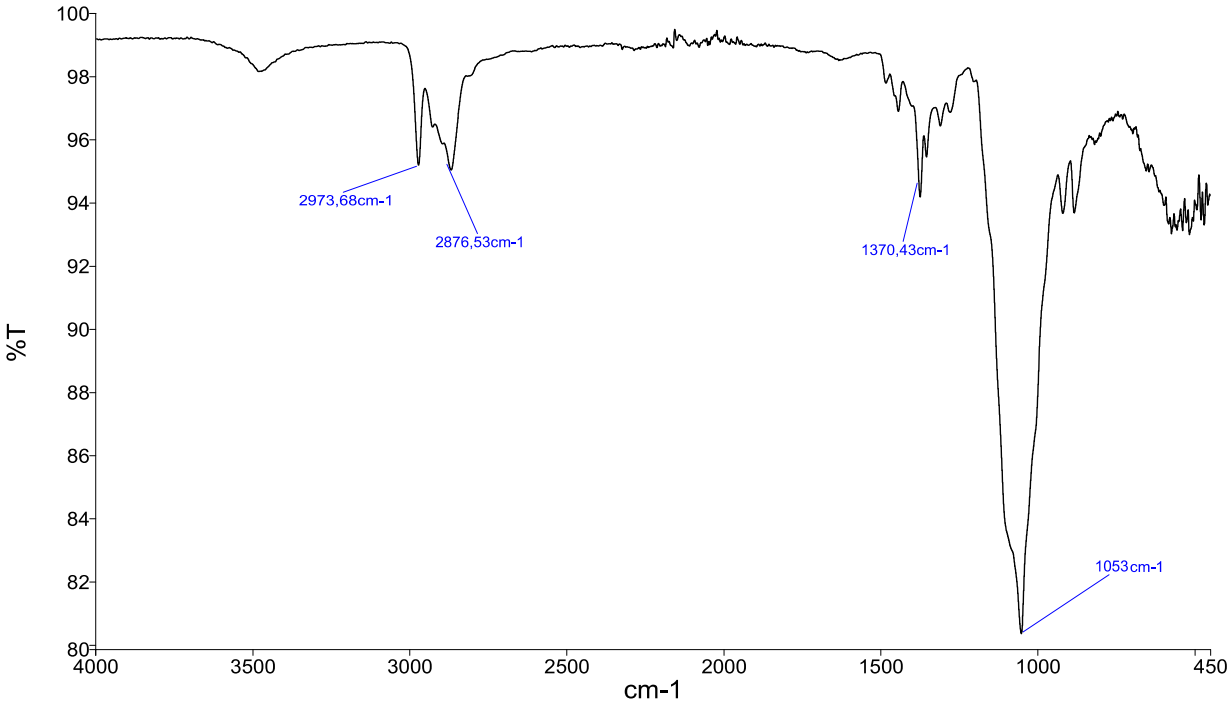

(b)

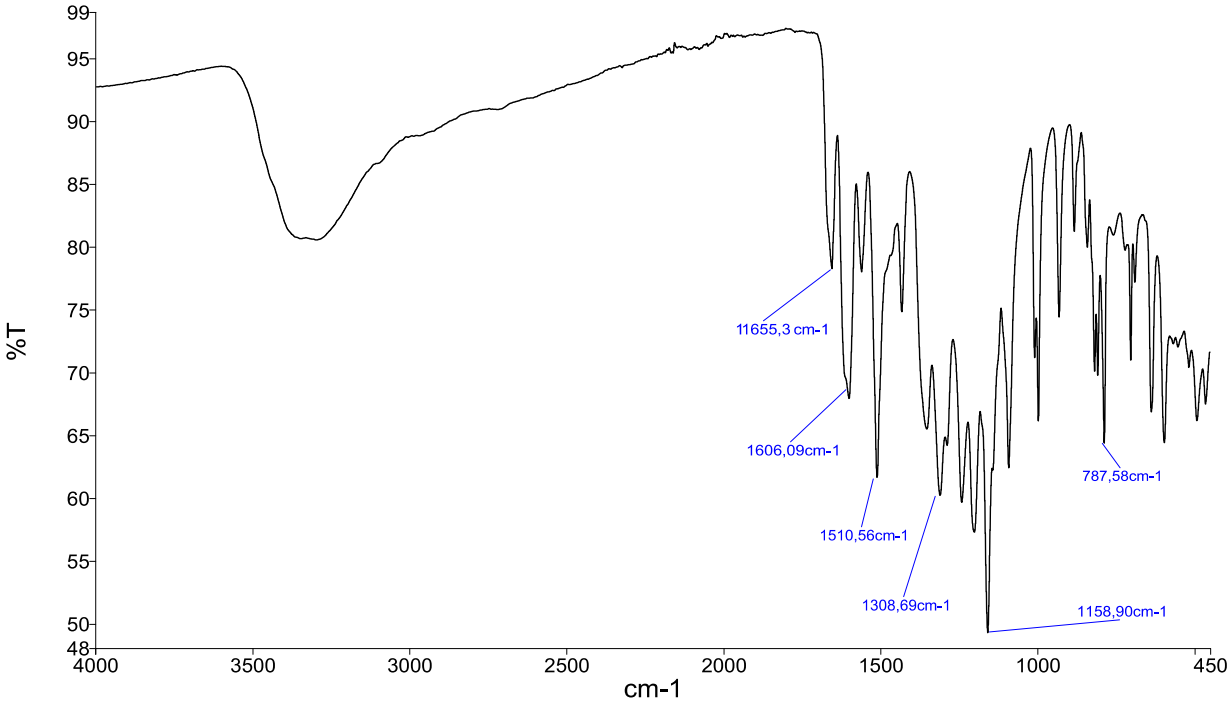

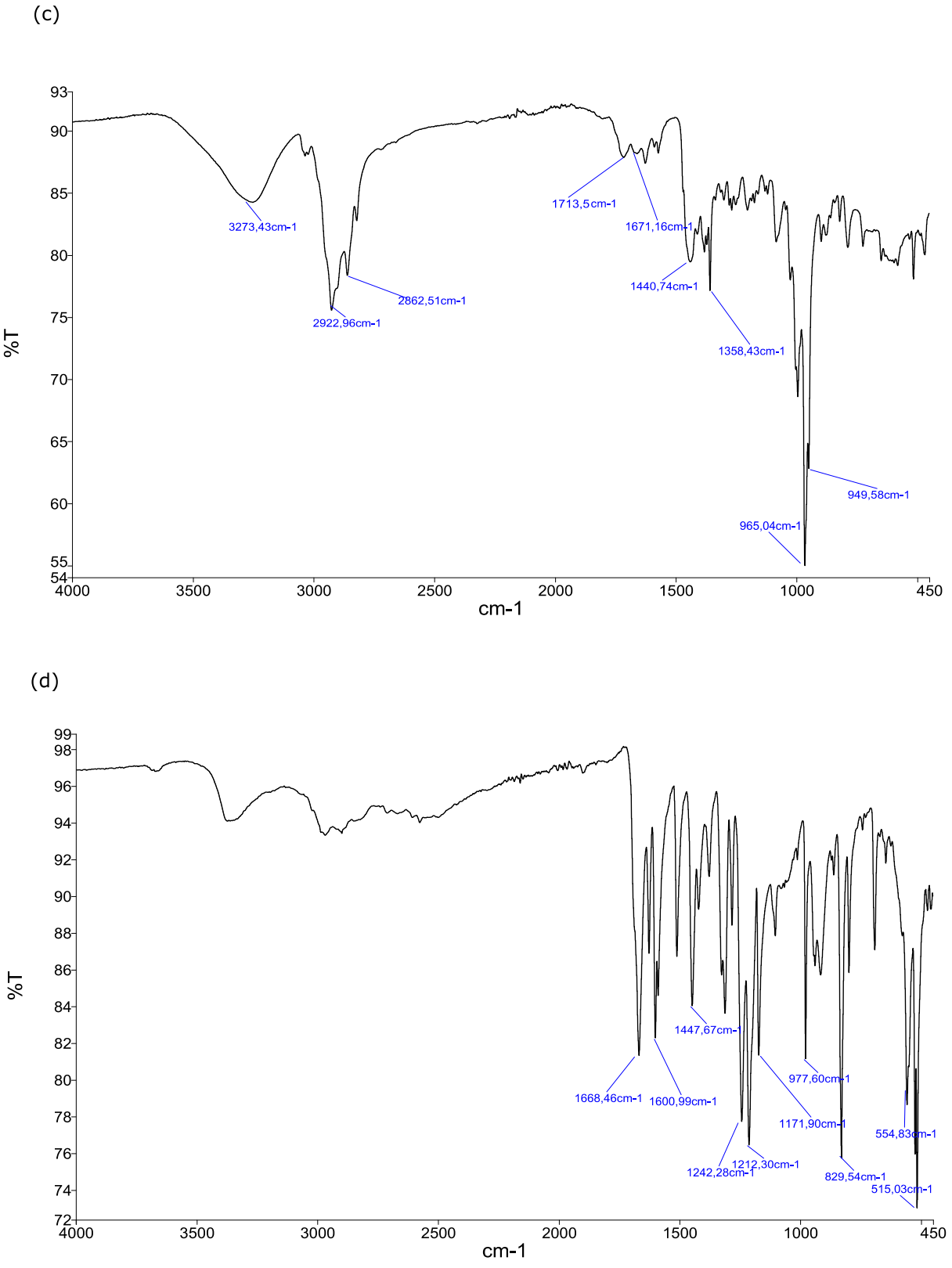

Figure C1: FTIR spectra of pure (a) EC, (b) quercetin, (c) retinol and (d) p-coumaric acid.